Alma Mater Studiorum – Università di Bologna

DOTTORATO DI RICERCA IN

Biologia Cellulare e Molecolare

Ciclo XXX

Settore Concorsuale di afferenza: 05/E2

Settore Scientifico disciplinare: BIO/11

TITOLO TESI

Cadherin 6 regulates Epithelial Mesenchymal Transition by restraining autophagy and controlling metabolism in metastatic thyroid cancer

Presentata da: Mila Gugnoni

Coordinatore Dottorato

Prof. Giovanni Capranico

Supervisore

Prof. Davide Carlo Ambrosetti

Co-supervisore

Dott.ssa Alessia Ciarrocchi

Esame finale: aprile 2018

Index

Abstract

The transdifferentiation of epithelial cells toward a mesenchymal phenotype (EMT) is a multi-step process fundamental for tumor cells to leave the primary lesion and colonize ectopic sites. Cadherins are structural proteins that play a pivotal role in transducing extracellular signals, regulating many cellular pathways. The molecular mechanisms which guide these signaling functions are far to be fully characterized. Cadherin-6 (CDH6) is a type-2 cadherin known to drive EMT during development and it is aberrantly re-expressed in some tumors. In thyroid cancer, CDH6 is a target of the TGFβ signaling and a marker of EMT, suggesting a role for this protein in the progression of this type of tumor. Papillary thyroid carcinomas (PTCs) are mostly indolent lesions, but in the 2-5% of cases this tumor metastasize. The identification of molecular markers that allow to distinguish, at the early stages of diagnosis, which tumors will behave aggressively, would be strategic to develop more specific anticancer approaches. In this work, we assessed the role of CDH6 in the metastatic progression of thyroid cancer and evaluated the transcriptional re-programming following TGFβ signaling. We observed that CDH6 knock-down changes cellular morphology and cell-cell interaction structures, partially reverting the EMT program in thyroid cancer cells. Searching for CDH6 interactors using a yeast two-hybrid screening approach based on a thyroid cancer patients library, we found GABARAP, BNIP3 and BNIP3L/Nix. Through these direct interactions, CDH6 restrains autophagy and induces DRP1-mediated mitochondrial fission. CDH6 not only affects mitochondrial structure but also controls cell metabolism. Indeed, CDH6-mediated mitochondrial fission is required to provide spared mitochondria to promote a highly energetic profile, needed for cell motility and invasion. Analysis of CDH6 cytoplasmic LIR domains suggests that many cadherin family members could associate to autophagic machinery regulating the process. The analysis of CDH6 expression in a cohort of human PTCs showed that CDH6 expression is strongly associated

with metastatic behavior and worse disease free survival probability of the patients. Moreover, CDH6 expression is up-regulated specifically in the cells undergoing EMT and leaving the primary site of the tumor. Finally, we attempted to discover new coding and non-coding regulatory elements mediating TGFβ-induced EMT in thyroid cancer cells.

<u>Introduction</u>

Thyroid Cancer

Thyroid cancer is the most frequent malignant disease of the endocrine system. Incidence rate varies by geographic area, age, and sex, generally it is three to four times higher in women than in males, and very low in children under 15 years old (1,2). The massive increase in newly diagnosed cases in the last decades is largely due to new sophisticated screening technologies which identify asymptomatic and indolent lesions not detectable with previous methods, indeed mortality rates remained unchanged (3).

Most thyroid cancers originate from the transformation of thyrocytes, epithelial cells which secrete the thyroid hormone, while medullary thyroid carcinomas are rare and originate from the transformation of the calcitonin hormone-secreting C cells (4).

The three mayor histotypes in thyrocytes-derived cancer are defined by the level of cell differentiation, which is a classical parameter to distinguish aggressiveness at the time of the diagnosis. Well-differentiated thyroid tumors maintain morphological features of cells of epithelial origin and are usually characterized by slow proliferation and low metastatic spreading, and a 5-year survival higher than 95% (1). By contrast, anaplastic tumor cells are morphologically undifferentiated, tend to form widely infiltrative masses and spread to regional and ectopic sites, with a median 1-year survival rate inferior to 10-20% (Figure 1) (5,6).

It has been established that activating mutations in the proteins of Mitogen-activated protein kinase (MAPK) pathway favor thyroid tumorigenesis. In the recent years, a lot of studies tried to establish if mutations within this pathway (like BRAF V600E) could be used as prognostic factors (6,7). However, the association of these mutations with the metastatic behavior of these tumors has not clearly been demonstrated (7). Exploring the molecular differences between low and high aggressive

thyroid tumors would be of great importance to understand the basis of thyroid tumorigenesis and likely to improve patients' treatment and management.
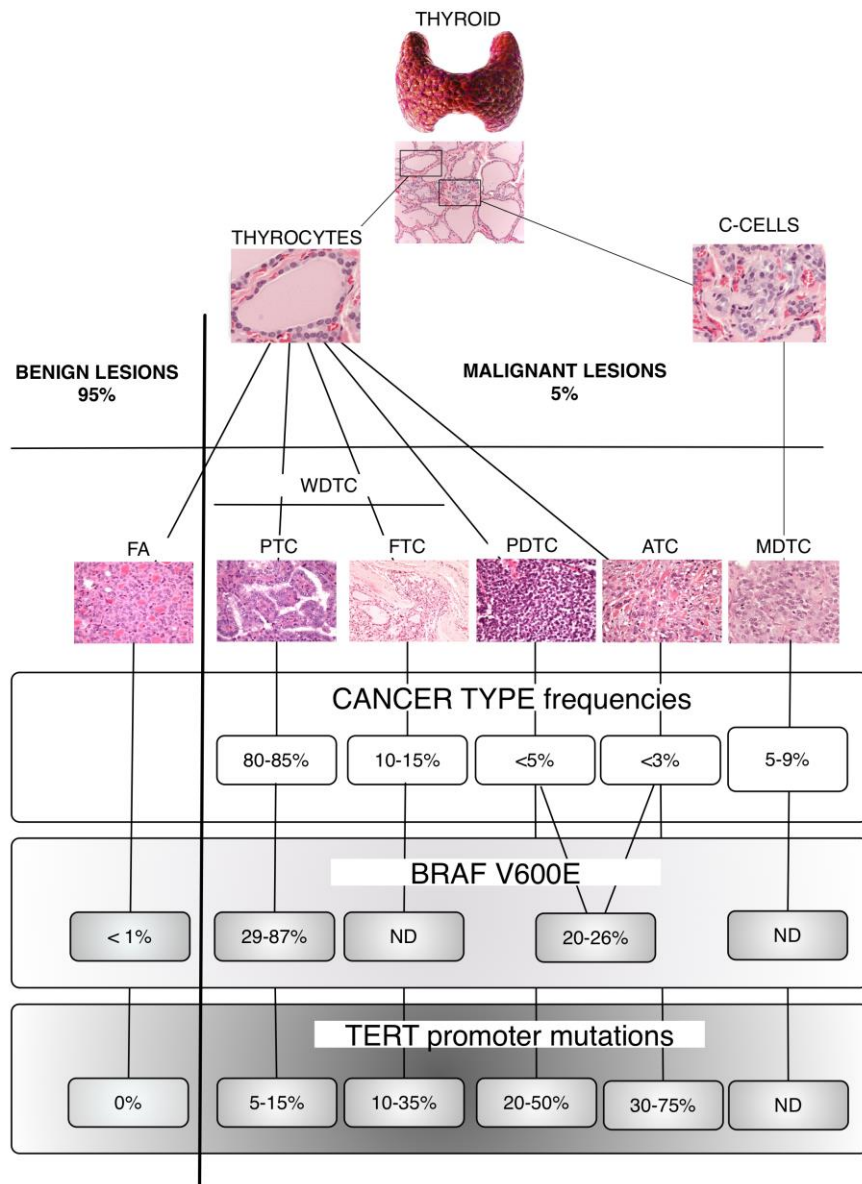
Figure 1. Schematic representation of thyroid tumor histotypes and BRAF V600E and TERT promoter mutations frequency in benign and malignant lesions. Most thyrocytes-derived lesions are benign follicular adenomas (FA). The malignant lesions, based on cell differentiation, can be divided into well-differentiated (WDTC), poorly differentiated (PDTC) and anaplastic (ATC) thyroid carcinomas. Among the WDTCs, papillary thyroid carcinomas (PTC) and follicular thyroid carcinomas (FTC). From C cells transformation originates medullary thyroid carcinoma (MDTC). IHC images magnification 200X. ND= not detected.

Papillary Thyroid Carcinoma (PTC)

Figure 1 shows the major histotypes of thyroid cancer. Among the well-differentiated lesions, the papillary thyroid carcinoma (PTCs) is the most common, accounting for 65-93% of all thyroid tumors, depending on the geographic area (1). PTC is generally an indolent lesion. However, 2-5% of these tumors present distant metastases leading to negative outcome of the patients (8,9). Diagnosis and prognosis for these tumors are based exclusively on morphological characteristics, which reflects the limited knowledge of the molecular mechanisms that control cell transformation and tumor progression in thyroid tumors.

Indeed, due to the lack of markers which can discriminate between aggressive and indolent forms of PTCs, the great majority of patients are surgically treated with total thyroidectomy, lymph node neck dissection and, in some cases, with radioiodine ablation (RAI) (10).

The role of genetic factors in this type of tumor is not completely clear (2,7). Based on the tumor cancer genome atlas (TCGA) results, PTCs present the lowest incidence of mutations among all solid cancers (11). Several mutually exclusive genetic alterations which lead to MAPK pathway activation have been described as frequent in this tumor (12,13). Point mutations (mainly in BRAF and NRAS) are found in more than 75% of PTCs, gene fusions in 15% and copy number variations in 7% of cases (11). The most common chromosomal rearrangement in PTCs involves the Rearranged During Transfection (RET) (gene and results into fusions RET-PTC) involving Neurotrophic Receptor Tyrosine Kinase 3 (NTRK3), Neurotrophic Receptor Tyrosine Kinase 1 (NTRK1), Anaplastic lymphoma kinase (ALK) and other kinases of the MAPK pathway.

PTC progression has been associated with mutations in genes as Tumor Protein p53 (TP53), Phosphatidylinositol-4,5-Bisphosphate 3-Kinase Catalytic Subunit Alpha (PIK3CA), AKT Reverse

Transcriptase (TERT) have been described as largely associated with high grade thyroid cancer (ATC and metastatic PTCs) (2,11,13).

Recently, a signature composed by the duplication of Chr1q, the duplication of TERT locus and the mutation on the TERT promoter, called Thyroid TERT Chr1q (THYT1), has been proposed as a predictive marker of distant metastases and reduced patients' survival probability (14).

To date, the discovery of new markers associated with aggressiveness of PTC is still a major challenge.

Epithelial to Mesenchymal Transition (EMT)

To leave their original site and spread to adjacent or distant tissues, epithelial tumor cells must undergo a profound molecular reorganization to modify their epithelial characteristics, including cell-cell adhesion, polarity, lack of structures for motility, and acquire mesenchymal features which allow migration, invasiveness and resistance to apoptosis (15). This complex and reversible process is fundamental in cancer metastasization and in non-pathological processes, like embryonic development, and it is known as epithelial-mesenchymal transition (EMT). The reverse of this program, the mesenchymal-epithelial transition (MET), is equally important in the subsequent migration phases, to allow cells to re-differentiate and colonize ectopic sites (16).

During EMT, polarized and non-motile epithelial cells, embedded in a well-organized and interconnected network, must dramatically change their molecular profile, starting from the adhesion molecules present on the plasmatic membrane which guide cell-cell interaction and cytoskeleton asset.

Following a driving signal (e.g. TGFβ or other growth factor), EMT initiation leads to the activation of a transcriptional program which involves the up-regulation of many transcription factors (Figure

2). This results in the inhibition of epithelial proteins expression, including those participating to cell-cell interaction and to the induction of mesenchymal proteins, which potentiate the ability of the cells to interact with the extracellular matrix favoring cell movement (Figure 2b) (17,18).

Even though variations in EMT-associated gene expression program are dependent on cell and tissue type, the switch from epithelial to mesenchymal cadherins on cell surface is one of the main hallmarks of the process (17).
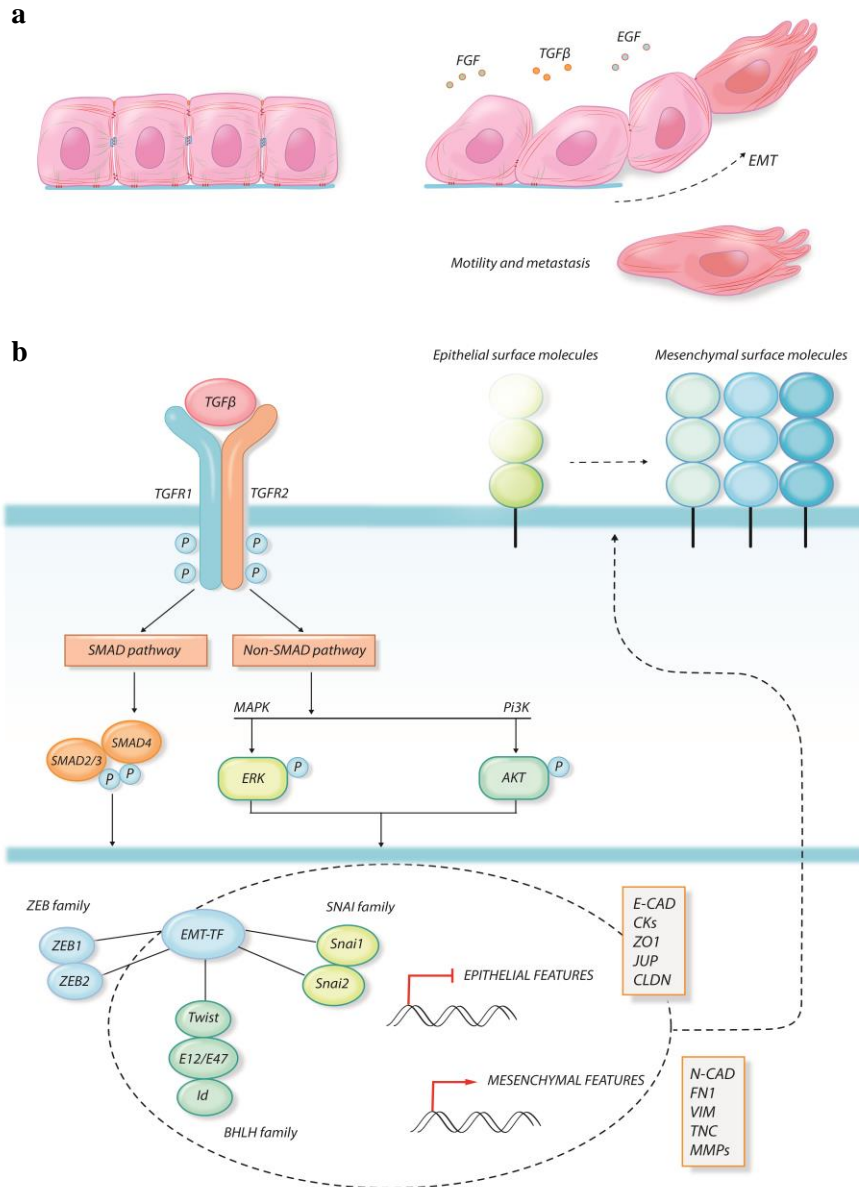
Figure 2. Representation of EMT process. **a**. Changes in cellular polarity, cell-cell interaction and cell morphology following EMT induced by growth factors signaling like TGFβ, Fibroblast Growth Factor (FGF) and Epidermal Growth Factor (EGF). **b.** Schematic illustration of SMAD and Non SMAD-mediated TGFβ cascade in cancer. TGFβ receptors (TGFR1/TGFR2) are activated and phosphorylate SMAD2/3, which associate to SMAD4.The complex translocate into the nucleus to control the expression of a network of mesenchymal genes. The MAPK and Phosphatidylinositol-3-Kinase (PI3K)-class I pathways can be directly activated by TGFβ and regulate EMT-related transcription factors (TFs) like Snail Family Transcriptional Repressor 1 and 2 (SNAI1 and 2), Zinc Finger E-Box Binding Homeobox 1 and 2 (ZEB1 and 2), Twist Family BHLH Transcription Factor (TWIST), E-proteins (E12/E47) and the repressor Inhibitor of DNA Binding 1 (Id). The reorganization of genome transcription is at the base of the change in the organization of adhesion molecules on the cell membrane, which dictates the rules of cell-cell adhesion and influences cytoskeleton structure and stress fibers formation.

10

Cadherins

The cadherin superfamily is composed by over 100 transmembrane proteins involved in the organization of cell-cell adhesion junctions which dictate the specificity of cellular interactions (19,20). E-cadherin (CDH1, E-CAD) and N-cadherin (CDH2, N-CAD) are the prototypes and by far the most studied members of the cadherin family (Table 1, Figure 3). During EMT, epithelial cadherins such as E-CAD, are displaced by the multiprotein complexes at the adherent junctions and are substituted by mesenchymal cadherins, such as N-CAD (21). This switch relapses on the protein complexes which connect cadherins to the cytoskeleton and triggers its rearrangement and the formation of lamellipodia and filopodia, actin protrusions for cell movement. It is reported that metastatic cells are enriched in filopodia-like structures and that their presence correlates with invasiveness (22).

Identified as cell membrane-associated Ca^{2+}-dependent glycoproteins, cadherins' role is not confined to cell-cell recognition and adhesion, but extends to signal transduction to regulate cell growth, fate and behavior (21).

Evidence indicates that different cadherins play non-redundant roles and it is commonly believed that such large variability originates from the need of complex organisms to specifically differentiate intercellular interactions. Despite this, the potential role of cadherins other than the E- and N-CAD in cancer development and progression is a topic of great interest not yet fully explored.

Table 1

Family	Subfamily	Genes Names
Cadherins	Type I	CDH1, CDH2, CDH3, CDH4, CDH15
	Type II	CDH5, CDH6, CDH7, CDH8, CDH9, CDH10, CDH11, CDH12, CDH18, CDH19, CDH20, CDH22, CDH24
	7D	CDH16, CDH17
	Desmosomal	DSC1, DSC2, DSC3, DSG1, DSG2, DSG3, DSG4
	Flamingo/CELSR	CELSR1, CELSR2, CELSR3, CDH13, CDH26
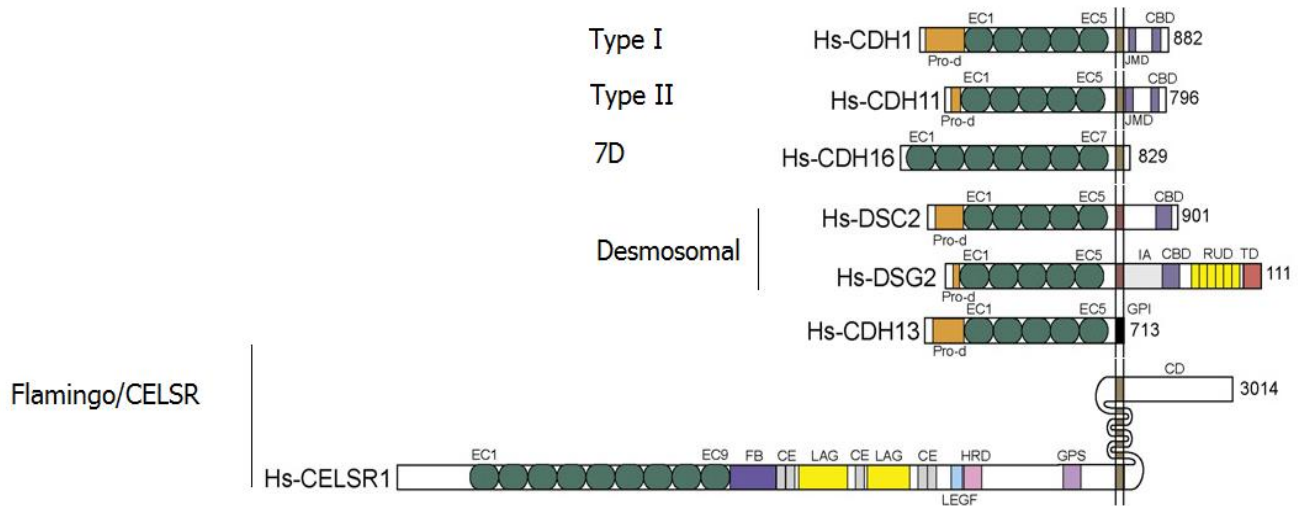
Figure 3. Schematic representation of the human cadherin family. The proteins' structure is aligned at transmembrane domain and shown to scale. The numbers displayed on the right refer to the total number of amino acid residues. Domains legend: CBD: cadherin-specific catenin binding domain; CD: cytoplasmic domain; CE: cysteine-rich EGF repeat-like domain; EC: extracellular repeat; FB: Flamingo box; GPI: glycosyl phosphatidyl inositol anchor; GPS: latrophilin/CL-1-like GPS domain; HRD: hormone receptor domain ; IA: intracellular anchoring domain; JMD: juxta membrane domain; LAG: laminin A globular domain; LEGF: laminin-type EGF-like domain; Pro-d: prodomain; RUD: intracellular repeated unit domain; TD: terminal domain.

The expression of specific cadherins is tightly regulated during embryogenesis, cell differentiation and maintenance of different tissues and organs. Given the broad spectrum of their functions, it is not surprising that their aberrant expression and function have been linked to cancer progression and metastasization (23,24).

In many epithelial cancers, loss of E-CAD is correlated to increased invasiveness and is usually accompanied by the up-regulation of N-CAD, underlying the EMT program activation (25). N-CAD can associate with fibroblast growth factor receptor (FGFR) and promote the translocation and activity of β-catenin in the nucleus, sustaining tumor progression. Nevertheless, it would be misleading to think that N-CAD is always correlated with bad prognosis, indeed, in neuroblastoma, its down-regulation is associated with metastases (26). Cadherin3 (P-CAD) activity is tumor type-specific. In some cancer cells, it plays a tumor suppressor role, replacing E-CAD (27). In other contexts, it can bind to insulin-like growth factor 1 receptor (IGF1R) activating p120-catenin promoting cell migration and invasion (28). Cadherin17 (LI-CAD) promotes gastrointestinal tumors metastasization while cadherin5 (VE-CAD), following N-CAD up-regulation, promotes tumor spreading (29,30). Cadherin13 (T-CAD) loss enhances epidermal growth factor receptor (EGFR) signaling, thus promoting carcinoma progression (31). Protocadherin's loss is common in some types of tumor, and considered a hallmark of increased aggressiveness, while in breast cancers the expression of protocadherin7 (PCDH7) is correlated to cell proliferation and migration (Figure 4) (32).
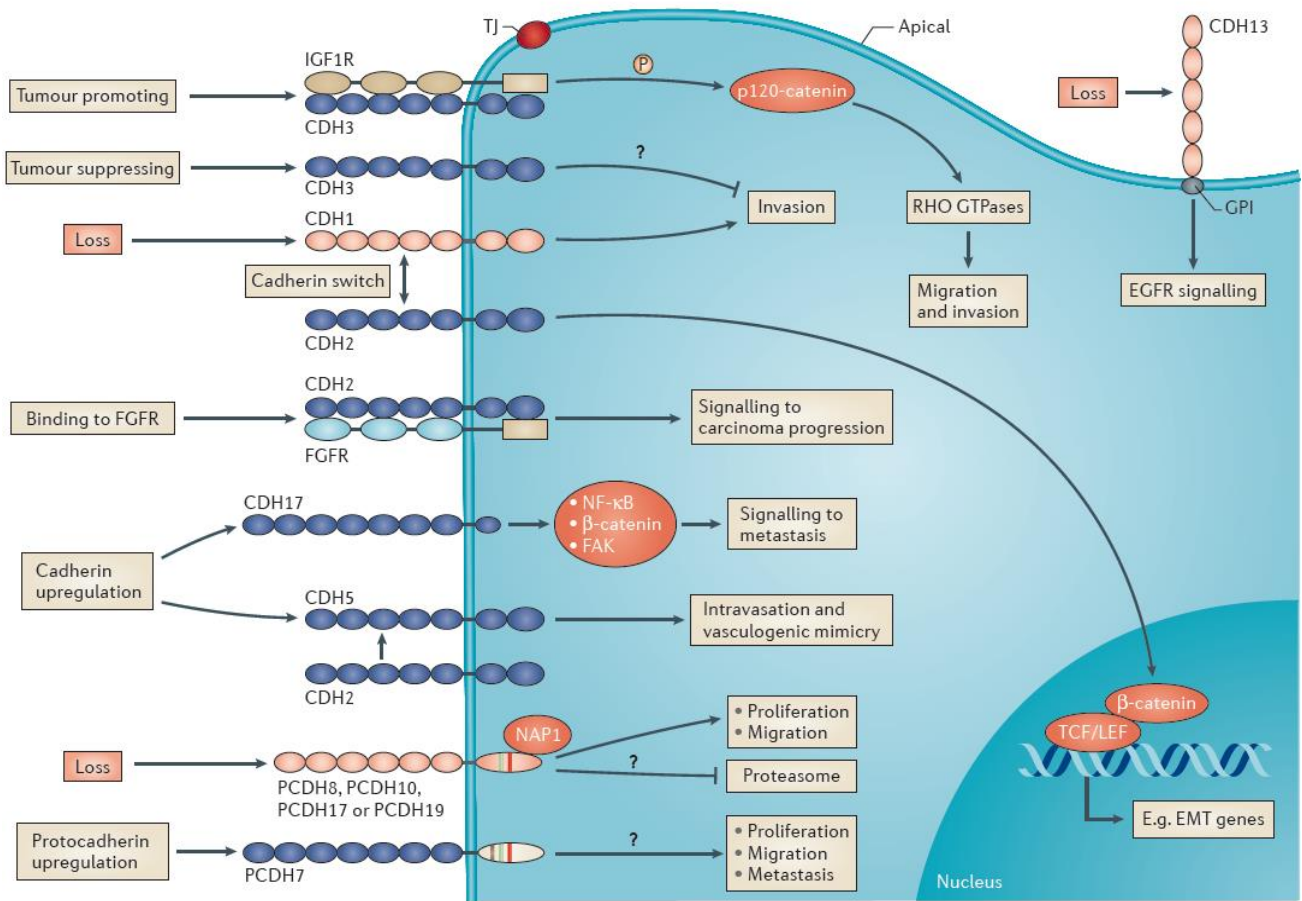
Figure 4. Molecular interaction of some representative cadherin superfamily members in cancer. Putative mechanisms not yet established are signaled with question marks.

Legend: FAK: focal adhesion kinase; GPI: glycosylphosphatidylinositol anchor; NAP1: NCK-associated protein 1; NF-κB: nuclear factor-κB; TCF/LEF: T-cell transcription factor/lymphoid enhancer-binding factor; TJ: tight junction.

Cadherin 6

Cadherin 6 (CDH6, K-CAD) is a member of the Type II cadherin family, which partakes in the morphogenesis of central nervous system and kidneys during embryogenesis. In renal development, CDH6 controls the conversion of mesenchymal precursors into the epithelium of the developing nephrons (34-36). It is known that crucial players during embryogenesis are often re-expressed in cancer progression and CDH6 confirms this paradigm. Indeed, CDH6 overexpression has been described in ovarian cancer and renal carcinoma (37-40). In the latter, CDH6 expression strongly correlates with aggressive behavior and poor patient outcome. Analysis of the gene expression profiles available through The Cancer Genome Atlas (TCGA, portal website http://cancergenome.nih.gov) confirmed that CDH6 expression is tumor type dependent and enriched in these two types of cancer (Figure 5).
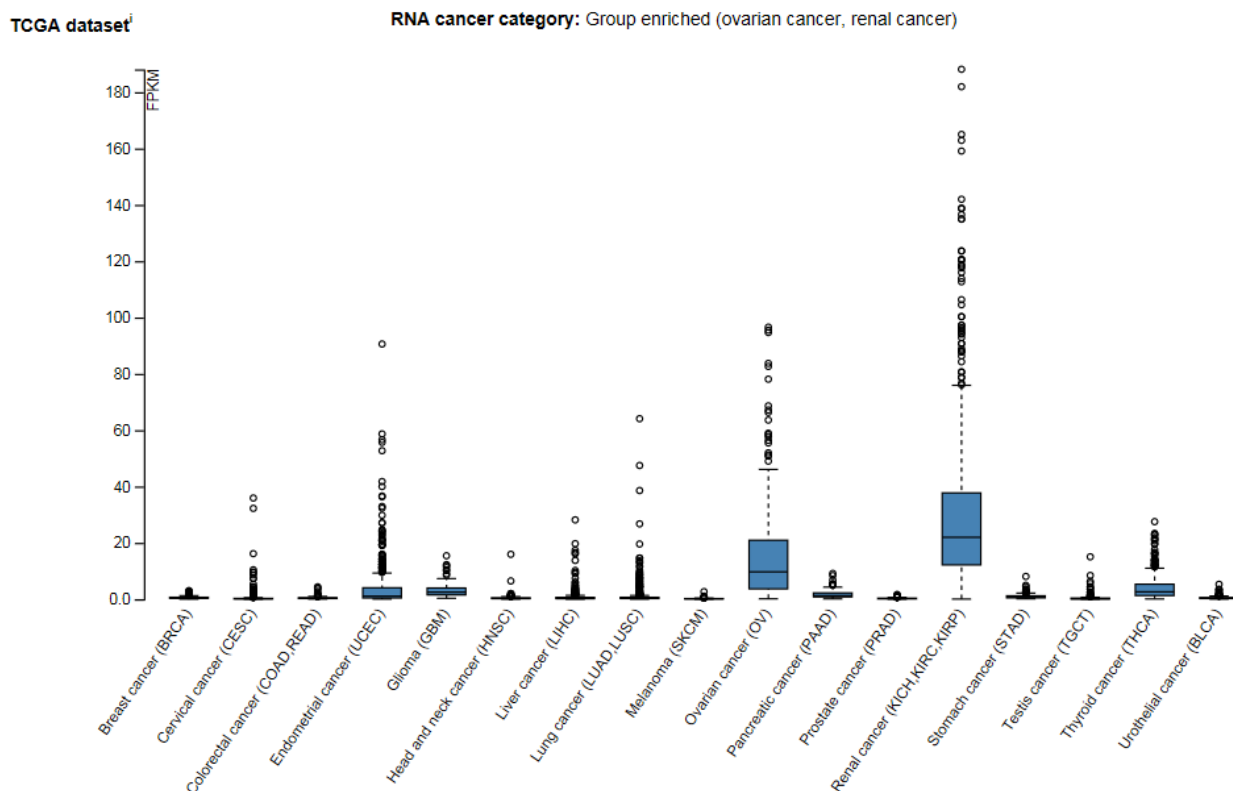
Figure 5. Cadherin6 expression in different cancer types from The Cancer Genome Atlas (TCGA) database. RNA enrichment is reported for Renal and Ovarian cancer.

Previous data from our laboratory demonstrated that in thyroid cancer cells, CDH6 is up-regulated following TGFβ oncogenic signaling. CDH6 in human is encoded by *cdh6* gene located on the short arm of chromosome 5, in cluster with other cadherins, in two main isoforms (long:L and short:S) (41). Both isoforms are highly expressed in PTC-derived cell lines BCPap and TPC1, compared to the thyrocytes-derived Nthy-ori-3.1 cell line (Figure 6a). Following TGFβ treatment, both isoforms are transcriptionally induced, in all three cell lines tested, but in a higher extent in thyrocytes-derived cell line, in which CDH6 basal expression is very low (Figure 6b) (42). The ID1-RUNX2 transcriptional axis partakes to the TGFβ-mediated CDH6 regulation during EMT (Figure 6c) (42,43). Given the highly specific and fundamental role of cadherins during cancer metastasization, these data suggest a potential role of CDH6 in mediating the progression of thyroid cancer.
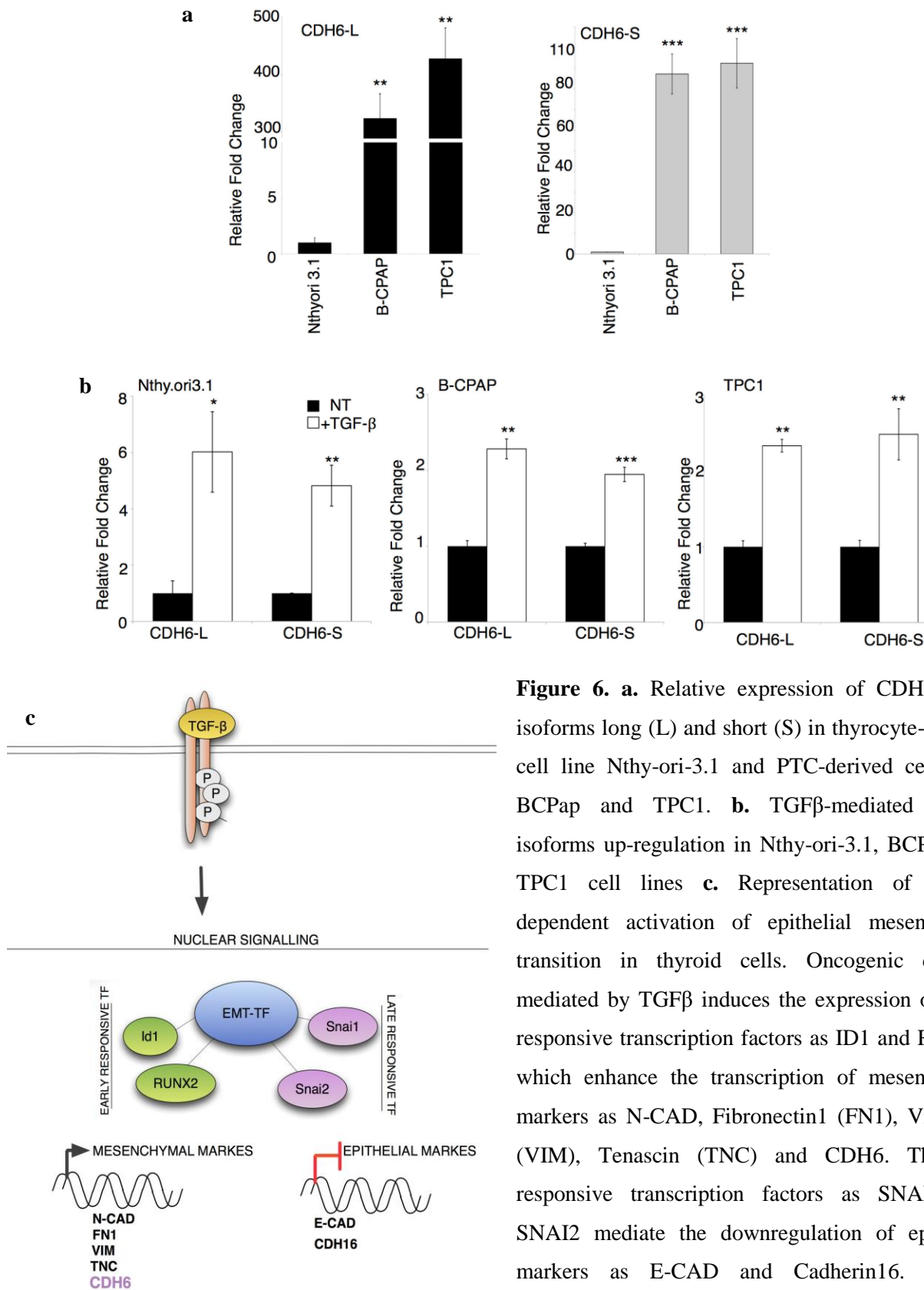
Figure 6. a. Relative expression of CDH6 main isoforms long (L) and short (S) in thyrocyte-derived cell line Nthy-ori-3.1 and PTC-derived cell lines BCPap and TPC1. b. TGFβ-mediated CDH6 isoforms up-regulation in Nthy-ori-3.1, BCPap and TPC1 cell lines c. Representation of TGFβ-dependent activation of epithelial mesenchymal transition in thyroid cells. Oncogenic cascade mediated by TGFβ induces the expression of early responsive transcription factors as ID1 and RUNX2 which enhance the transcription of mesenchymal markers as N-CAD, Fibronectin1 (FN1), Vimentin (VIM), Tenascin (TNC) and CDH6. The late responsive transcription factors as SNAI1 and SNAI2 mediate the downregulation of epithelial markers as E-CAD and Cadherin16. *P=0.05, **P=0.01. ***P=0.001.

17

Aim of the study

Regulatory factors selectively involved in tumor progression are promising candidates as molecular markers of aggressiveness at the time of diagnosis. The identification of these prognostic markers would provide clinicians with new tools to design the most appropriate approaches to thyroid tumor management. Based on our preliminary data, we hypothesize that CDH6 is a major determinant of the aggressive behavior of thyroid cancer and a crucial mediator of metastatic spreading. Thus, the goal of this project is to characterize the functional role of CDH6 in the progression of thyroid tumors and to dissect the signaling network centered on this protein. This project should also define whether CDH6 can be proposed as a new molecular marker of thyroid tumor aggressiveness in a clinical setting.

<u>Results</u>

CDH6 expression in PTC patients

Well-differentiated PTCs rarely develop distant metastases leading to negative patients outcome. The rarity of these lesions has so far limited the characterization of specific molecular mechanisms and the discovery of reliable markers to distinguish the aggressive PTCs from the indolent ones. To date, the presence of distant metastases at the time of diagnosis is the only prognostic factor of a negative outcome of the patients. Thus, to define whether CDH6 expression was associated with metastatic behavior of PTCs, a nested case-control study starting from the Thyroid tumor archive of our Institution was designed. It comprised over 2900 cases collected in the last 30 years, among which well differentiated PTC that developed distant metastasis (DM-PTCs) were searched. 50 DM-PTCs samples were recovered and 44 were available for the analysis. This represented one of the largest cohort of DM-PTCs ever analyzed. As control, 42 PTCs which did not metastasized (nm-PTCs), based on a minimum follow-up of 7-years, were selected (Figure 7). In these samples CDH6 expression was analyzed by IHC.
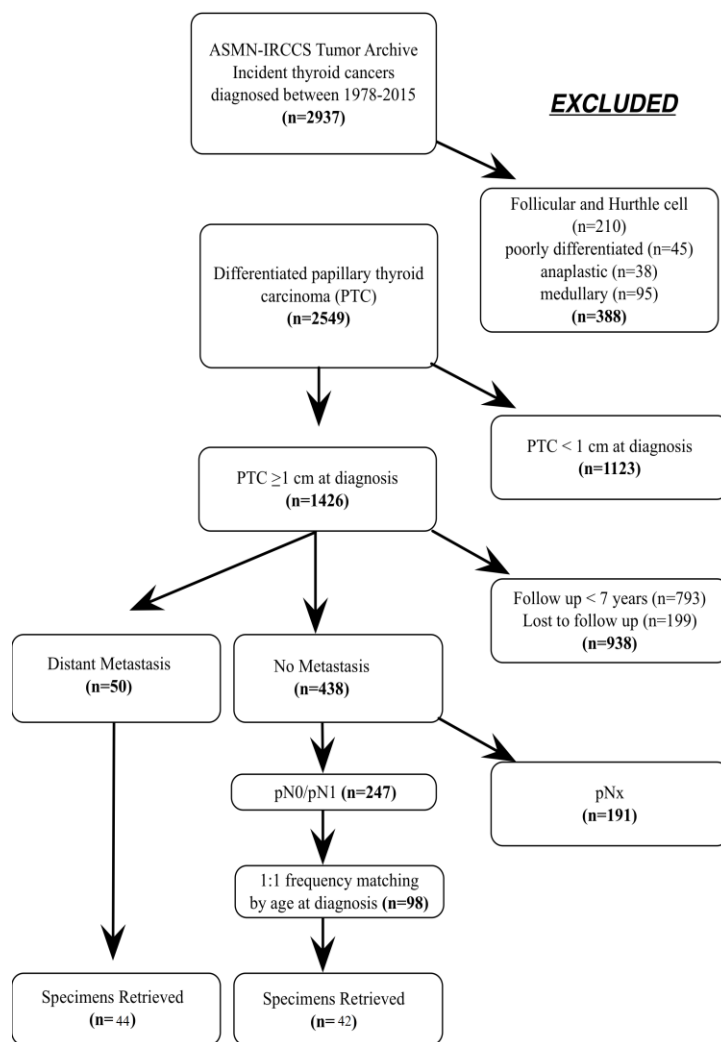
Figure 7. Diagram representing patients selection.

A strong correlation between CDH6 protein expression and the presence of distant metastasis was found. 43.2% of DM-PTCs (19/44) showed CDH6 positivity while only 16.7% (7/42) of non-metastatic, control PTCs were positive for CDH6 (p = 0.001) (Table 2). Furthermore, correlation of CDH6 expression with morphological and clinical variables showed that the expression of this cadherin within this cohort was strongly associated with reduced disease-free survival probability (Table 4, Figure 8a). Intriguingly, the same analysis limited to the DM-PTCs group indicated that CDH6 expression did not affect follow-up, indeed its expression was not associated with a worse course of the disease among the patients who developed distant metastases (Figure 8b). These results suggest that this cadherin is required specifically during the initial phases of metastatic spreading. Indeed, once tumor cells have reached the metastatic site, the mesenchymal features acquired through the EMT have to be reverted (through the mesenchymal-to-epithelial transition- MET) in order to allow metastatic cells to proliferate and colonize the site. Interestingly, in DM-PTCs, CDH6 expression was not homogeneous within the tumor, but restricted to clusters of cells interfacing the connective tissue at the invading front of the tumoral mass (Figure 8c-e). Morphologically, the CDH6-positive were completely different from the CDH6-negative tumor cells, displaying lengthened shape and not organized cell-cell adhesion structures, reminding of mesenchymal-like phenotype (Figure 8c-e). Noticeably, the analysis of the epithelial marker E-CAD showed that CDH6 positive cells retained E-CAD expression indicating that these cells have undergone a partial but not complete EMT (Figure 8c-e). All together, these features recall a well-known phenomenon, very important for cancer invasiveness and metastasization, named collective cell migration. Per se E-cadherin expression was highly homogenous within the samples analyzed without significant difference between DM- and control-PTC and did not correlate with any of the clinical and morphological features taken into consideration (Table 3, 5).

TABLE 2. CDH6 staining in PTC

	0 (Negative)	1 (<5 % positive cells)	2 (5-10% positive cells)	3 (>10% positive cells)	Chisq test
DM-PTC	25 (0.57)	0	7 (0.16)	12 (0.27)	*0.001*
Control-PTC	35 (0.83)	2 (0.05)	5 (0.12)	0	
LNM-PTC	19 (0.95)	0	1 (0.05)	0	0.13
noMet-PTC	16 (0.73)	2 (0.09)	4 (0.18)	0	
TOTAL	60 (0.70)	2 (0.02)	12 (0.14)	12 (0.14)	

Legend: DM-PTC = papillary thyroid cancer with distant metastases; LNM-PTC = PTC with local lymphnodal metastases; noMet-PTC = PTC without metastases

TABLE 3. ECAD staining in PTC

	0 (Negative)	1 (<50% positive cells)	2 (50-80% positive cells)	3 (>80% positive cells)	Chisq test
DM-PTC	0	2 (.05)	3 (.06)	41 (.89)	*0.47*
Control-PTC	0	2 (.05)	6 (0.15)	33 (.80)	
LNM-PTC	0	2 (.10)	3 (.15)	15 (.75)	*0.15*
noMet-PTC	0	0	3 (.14)	18 (.86)	
TOTAL	0	4 (.05)	9 (.10)	74 (.85)	

Legend: DM-PTC = papillary thyroid cancer with distant metastases; LNM-PTC = PTC with local lymphnodal metastases; noMet-PTC = PTC without metastases
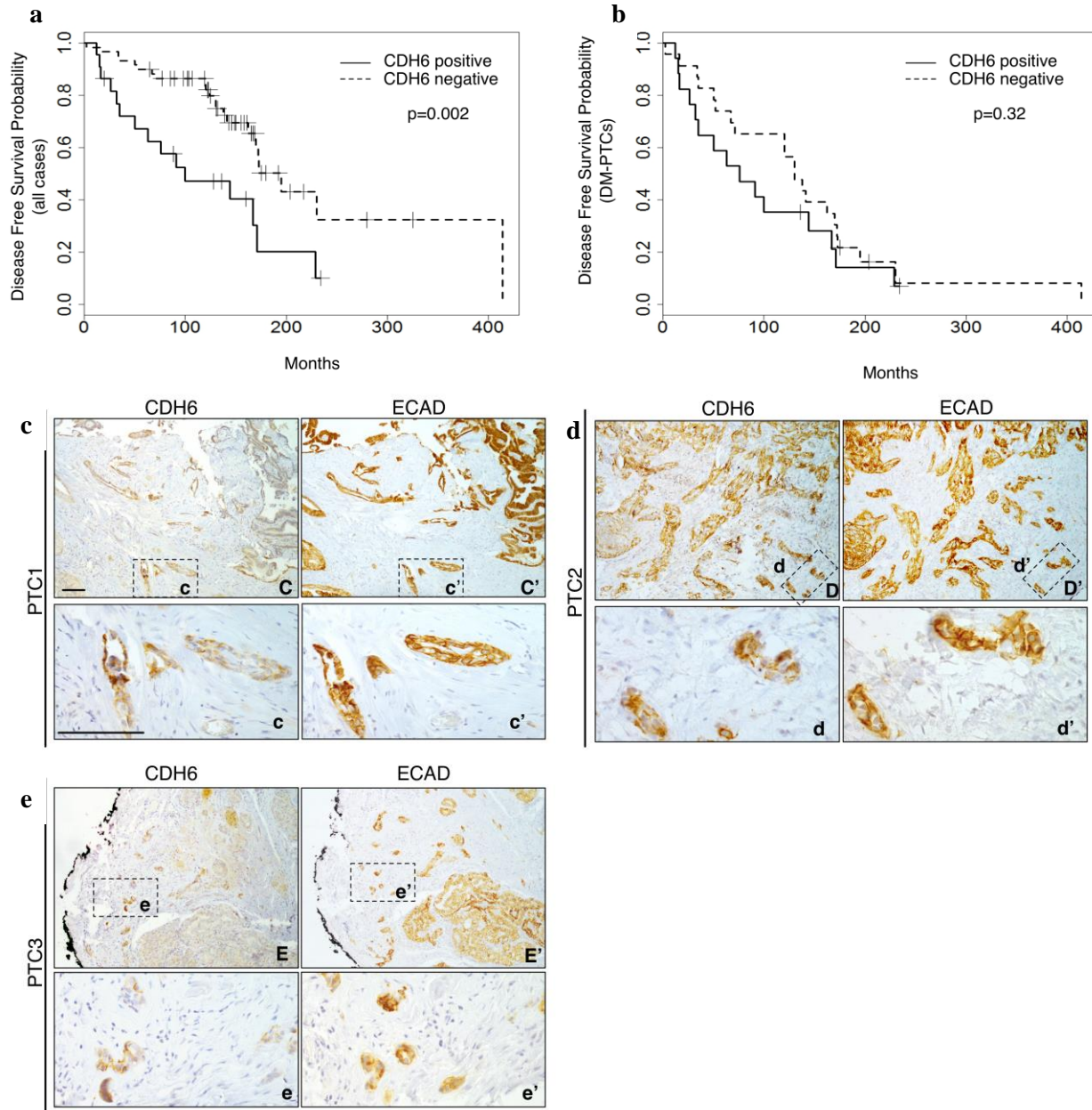
Figure 8. a,b. Kaplan-Meier curves showing disease-free survival probability correlated with CDH6 expression, on the complete PTC cohort analyzed (n=86, **a)** and among the DM-PTC samples (n=44, **b**). **c-e**. Immunohistochemistry detection of CDH6 and E-CAD expression in three DM-PTCs samples. Lower cases represent magnification of the upper images. Scale bar 100 μm.

TABLE 4. Association between CDH6 staining and clinical features in DM-PTCs

DM PTCs		CDH6 Negative n=25	CDH6 Positive n=19	P-value
Age at diagnosis, y		60.3 ± 16.1	50.0 ± 21.1	0.07
Sex				1
	Females	15 (.60)	12 (.63)	
	Males	10 (.40)	7 (.37)	
Histological Diagnosis				0.86
	CPTCs	13 (.52)	11 (.58)	
	TCV-PTCs	6 (.24)	5 (.26)	
	FV-PTCs	5 (.20)	2 (.10)	
	ST-PTCs	1 (.04)	1 (.05)	
pN				0.46
	0	2 (.08)	1 (.05)	
	1a	4 (.16)	6 (.31)	
	1b	19 (.76)	12 (.63)	
pT				0.30
	1b	1 (.04)	0	
	2	1 (.04)	2 (.10)	
	3	20 (.80)	12 (.63)	
	4a	2 (.08)	5 (.26)	
	4b	1 (.04)	0	
Pathologic Stage at Presentation				0.44
	I	1 (.04)	0 (.0)	
	II	3 (.12)	6 (.31)	
	III	3 (.12)	3 (.16)	
	IVa	14 (.56)	7 (.37)	
	IVb	4 (.16)	3 (.16)	
Follow Up Status				0.08

	NED	2 (.10)	2 (.12)	
	AWD	5 (.25)	10 (.59)	
	DOD	13 (.65)	5 (.29)	
	NA	5	2	
Lymph Node metastases				
	present	23 (.92)	18 (.05)	1
	absent	2 (.08)	1 (.95)	
Distant metastasis main site				
	lung	21 (.84)	15 (.83)	
	bone	2 (.08)	1 (.06)	
	mediastinum	2 (.08)	2 (0.11)	
Timing of Distant Metastases				0.31
	Synchronous	7 (.28)	9 (.47)	
	Metachronous	18 (.72)	10 (.53)	
ECAD staining				0.11
	Heterogeneous (<80% positive cells)	5 (.20)	0 (0)	
	Homogeneous (>80% positive cells)	20 (.80)	19 (1.0)	

CPTC: classic PTC, TCV-PTC: PTC, tall cell variant, FV-PTC: PTC follicular variant, ST-PTC: PTC solid trabecular, NED: no evidence of disease, AWD: alive with disease, DOD: dead of disease, NA: not available.

TABLE 5. Association between ECAD staining and clinical features in DM-PTCs

DM PTCs		*Heterogeneous ECAD staining <80% positive* n=5	*Homogeneous ECAD staining >80% positive* n=41	P-value
Age at diagnosis, y		59.6 ± 20.1	55.7 ± 18.9	0.67
Sex				1
	Females	3 (.60)	25 (.61)	
	Males	2 (.04)	16 (.39)	
Histological Diagnosis				0.91
	CPTCs	3 (.60)	21 (.51)	
	TCV-PTCs	1 (.20)	6 (.15)	
	FV-PTCs	0	2 (.05)	
	ST-PTCs	1 (.20)	12 (.29)	
pN				0.25
	0	0	5 (.12)	
	1a	0	10 (.24)	
	1b	5 (1)	26 (.64)	
pT				0.74
	1b	0	1 (.025)	
	2	0	3 (.07)	
	3	5 (1)	29 (.71)	
	4a	0	7 (.17)	
	4b	0	1 (.025)	
Pathologic Stage at Presentation				0.83
	I	0	1 (.02)	
	II	1 (.20)	8 (.20)	
	III	0	8 (.20)	
	IVa	3 (.60)	18 (.44)	
	IVb	1 (.20)	6 (.14)	
Follow Up Status				0.60
	NED	1 (.20)	3 (.08)	

	AWD	2 (.40)	13 (.34)	
	DOD	2 (.40)	22 (.58)	
	NA	0	3	
Lymph Node metastases				0.94
	present	0	5 (.12)	
	absent	5 (1)	36 (.88)	
Distant metastasis main site				0.54
	lung	5 (1)	32 (.80)	
	bone	0	3 (.08)	
	mediastinum	0	5 (.12)	
Timing of Distant Metastases				1
	Synchronous	2 (.04)	14 (.34)	
	Metachronous	3 (.06)	27 (.66)	

CPTC: classic PTC, TCV-PTC: PTC, tall cell variant, FV-PTC: PTC follicular variant, ST-PTC: PTC solid trabecular, NED: no evidence of disease, AWD: alive with disease, DOD: dead of disease, NA: not available.

CDH6 silencing changes cells morphology and architecture

Given the data obtained on patients samples, to define the relevance of CDH6 in the progression of PTC, its expression was selectively targeted with small-interference RNAs (siRNAs) on two cellular models of PTCs: TPC1 and BCPap cell lines. Transfection of CDH6 siRNA in both cell lines determined a profound downregulation of CDH6 expression both at mRNA and protein level (Figure 9a-c).
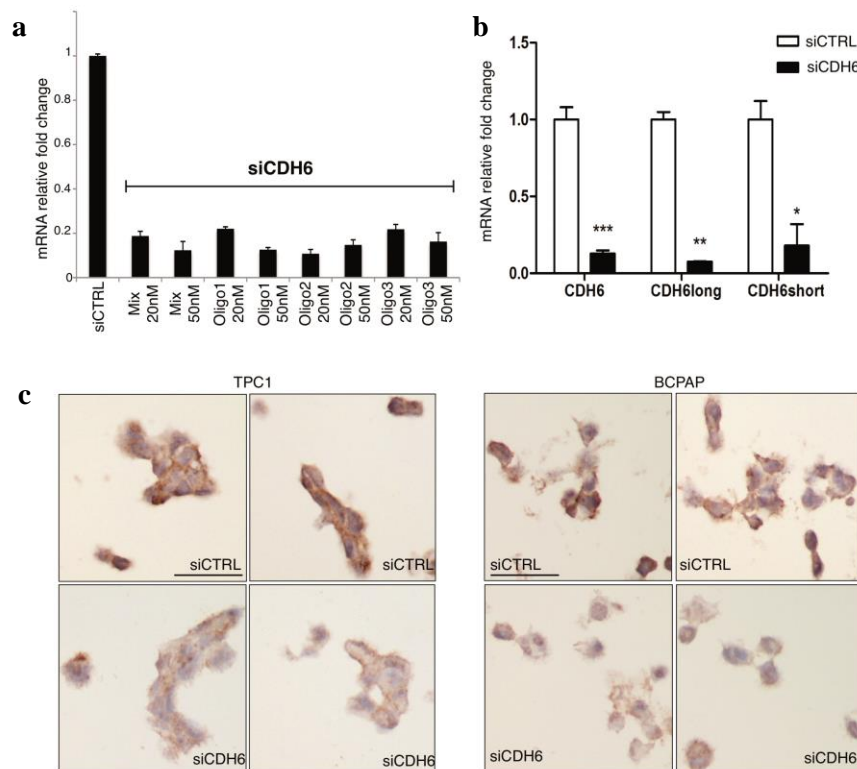
Figure 9 a. CDH6 silencing in TPC1 cell line. Relative expression of CDH6 in cells transfected with three different CDH6-targeting oligos alone or in combination compared to cell transfected with scramble oligos (siCTRL) ± s.d. **b.** Relative expression of CDH6 isoforms in TPC1 cell line transfected with control siRNA or CDH6 siRNAs **c.** Immunohistochemistry analysis of CDH6 expression in TPC1 and BCPap cell lines transfected with siCTRL or siCDH6. Magnification 40X. *P=0.05, **P=0.01, ***P=0.001.

Noticeably, CDH6 silencing profoundly affected cell morphology and cytoskeleton architecture (Figure 10a-c). Cell shape changed from well-defined to flat and blurred, with increased size

compared to control cells. Thus, in silenced cells plasmatic membranes were no longer distinguishable and cells resembled a uniform monolayer (Figure 10a). β-catenin staining unraveled a roof tile-like organization in cells silenced for CDH6, which is absent in control cells (Figure 10c). Actin filaments staining also revealed a profound effect on cytoskeleton organization upon CDH6 knock-down. Actin fibers running parallel to the membrane in control cells were rearranged forming thick fibers which crossed the cells and changed the structure of cell junctions, in CDH6 silenced samples (Figure 10b).
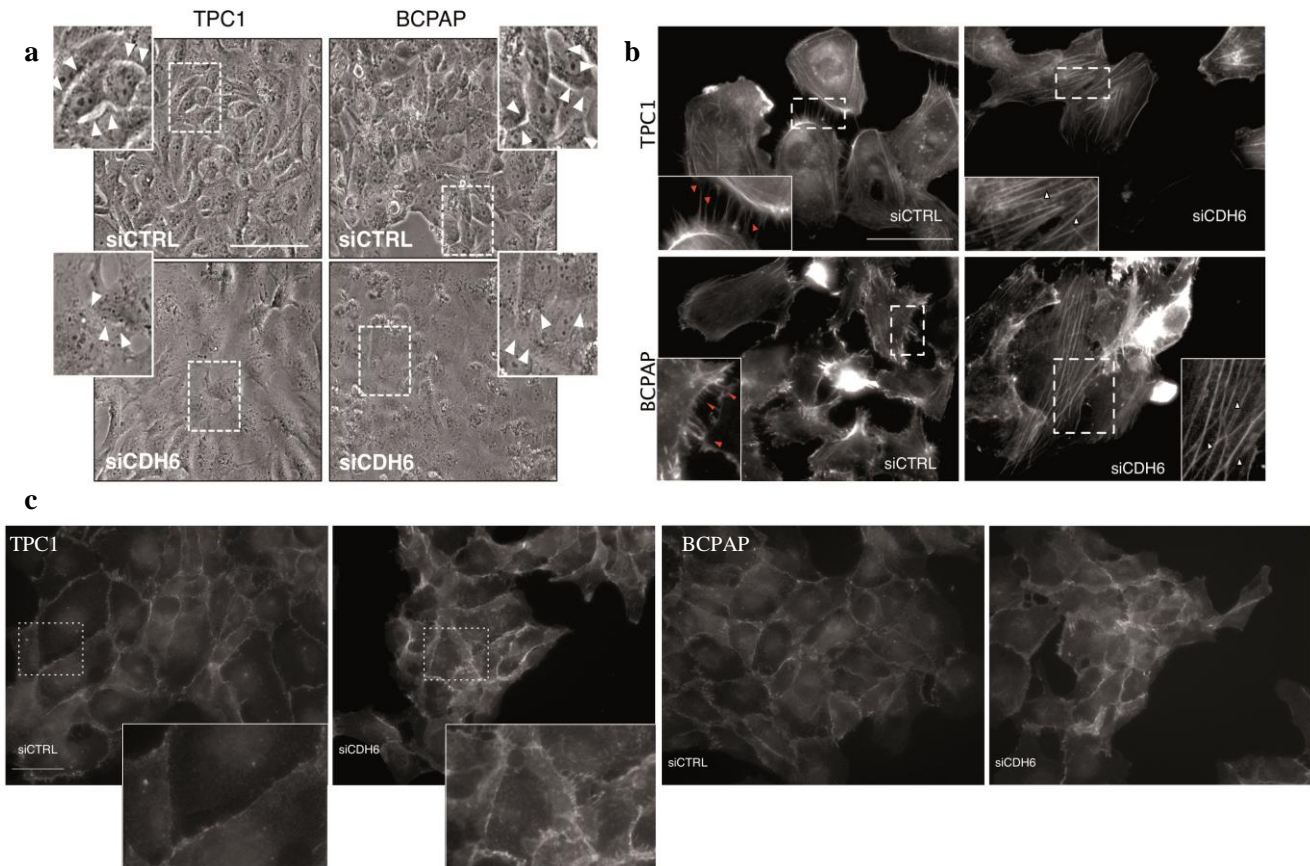
**Figure 10. a.** Optical microscope images of siCTRL or siCDH6 TPC1 and BCPap cell lines. Arrowheads indicate cell membrane cell-cell interaction. Scale bars, 100 μm. **b.** Phalloidin immunofluorescence staining to highlight actin filaments in siCTRL or siCDH6 cells. **c.** β-Catenin immunofluorescence staining to highlight cell membrane and cell-cell interactions in siCTRL or siCDH6 TPC1 and BCPap cell lines.

Moreover, in CDH6 silenced cells the density of cytoskeleton protrusions capable to sustain cell movement, like lamellipodia and filopodia, drastically diminished (Figure 10b). This kind of well-organized stress fibers were described in literature as a feature of non-migrant cells (44). This observed cytoskeleton rearrangement also affected cell-cell adhesion properties. Indeed, staining of phosphorylated-Focal adhesion kinase (p-FAK), a tyrosine kinase implicated in Integrin-mediated adherent junctions, showed a re-localization of this protein. p-FAK distribution changed from disperse and homogenous along the plasmatic membrane in control cells, to localized at the level of cell-cell junction in correspondence of the actin fibers nucleation centers in siCDH6 cells (Figure 11a). The involvement of cell junctions in the rearrangements induced by CDH6 knock-down was confirmed by the staining for the tight junction component ZO1 (45). Upon CDH6 silencing, ZO1 specifically relocated at the interconnection between adjacent cells, co-localizing with actin filaments (Figure 11b). In addition, FAK phosphorylation was profoundly inhibited by CDH6 silencing while ZO1 protein levels remained stable (Figure 11d).

CDH6 silencing reverts EMT program in PTC cell lines

Next, the potential role of CDH6 in defining the EMT phenotype of thyroid cancer cells was assessed. CDH6 silencing caused a significant down-regulation of the mesenchymal N-CAD but did not lead to changes in the classical epithelial E-CAD, which was not expressed in either siCDH6 or siCTRL cells (Figure 11c,d). By contrast, the epithelial CDH16 was transcriptionally up-regulated following CDH6 knockdown (Figure 11c). CDH16 was first discovered as a kidney-specific cadherin but was then found expressed in thyroid cells during development and down-regulated, in a higher extent compared to E-CAD, in thyroid transformed cells (46). The phenotype observed suggested that

CDH6 ablation was capable of partially revert the EMT phenotype of PTC-derived cell lines, influencing the expression and stability of genes and proteins involved in the process.
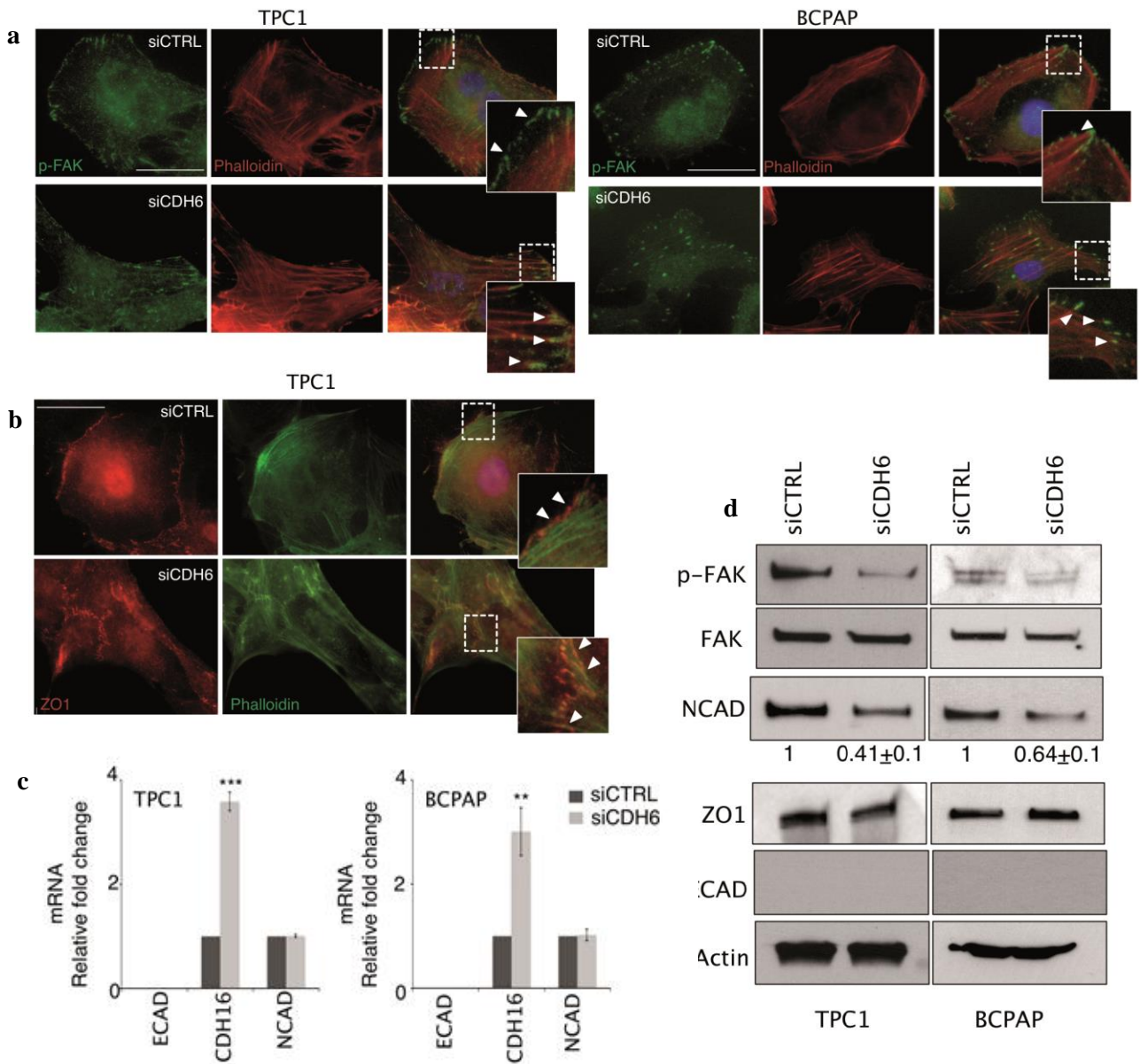
Figure 11. a. Phalloidin and p-FAK immunofluorescence staining of actin filaments in TPC1 and BCPap siCTRL and siCDH6 cells. **b**. Phalloidin and ZO1 immunofluorescence staining in TPC1 siCTRL and siCDH6 cells. Scale bars, 100 μm. **c.** qRT-PCR analysis of E-CAD, CDH16 and N-CAD expression in TPC1 and BCPap siCTRL and siCDH6 cells. **d.** Western blot analysis of total and p-FAK, N-CAD (quantification shows the percentage of N-CAD normalized on actin levels in siCDH6 compared to siCTRL cells ±s.d), ZO1 and ECAD in TPC1 and BCPAP cells. N° of replicates =3 *P=0.05, **P=0.01, ***P=0.001.

CDH6 silencing affects cell proliferation, invasion and migration

Strikingly, CDH6 silencing significantly inhibited cell proliferation, measured by growth curve (Figure 12a) and cell vitality (Figure 12b) in both cell lines tested. Accordingly, cell cycle evaluation with Propidium Iodide (PI) flow-cytometry staining showed a reduced number of cells in G1/S transition and a block in G0/G1, confirming an arrest in cell proliferation (Figure 12c).

Wound-healing and matrigel invasion chamber assays were used to evaluate CDH6-mediated cell migration and invasion. CDH6 silencing restrained the capacity of cell to migrate in both TPC1 and BCPap cell line and to invade the matrigel chambers in BCPap cell line (Figure 12d,e).

CDH6 controls autophagy

To get deeper knowledge on CDH6 molecular function, its interactors in human PTC samples were searched using a Membrane Yeast Two Hybrid assay. The full length CDH6 transmembrane protein was used as bait to search new interactors by screening a cDNA library obtained from 5 PTC patient samples. Before the screening, the library was normalized to allow the detection also of less represented protein that potentially interact with CDH6. From this analysis twelve proteins were identified. Unexpectedly, the most representative CDH6 interactors were the autophagy-related proteins Gamma-aminobutyric acid receptor-associated protein (GABARAP) and GABA Type A Receptor Associated Protein Like 2 (GATE16/GABARAPL2), and the outer mitochondrial membrane proteins BCL2 Interacting Protein 3 (BNIP3) and BCL2 Interacting Protein 3 Like (BNIP3L/Nix) (Figure 13).
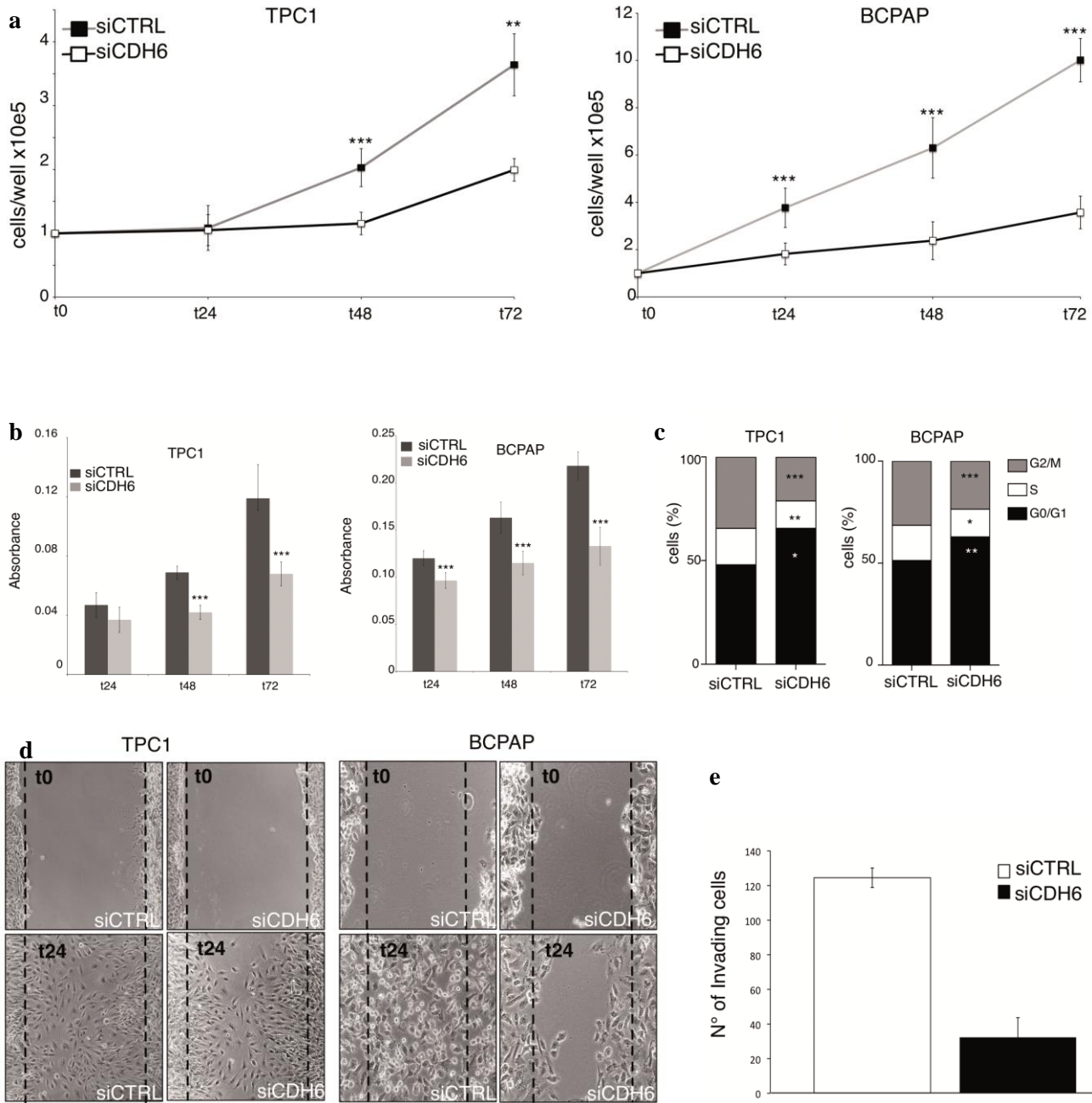
Figure 12. a. Cell proliferation assay in siCTRL and siCDH6 TPC1 and BCPap cell lines. **b.** MTT assay to evaluate cell vitality in siCTRL and siCDH6 TPC1 and BCPap cell lines. **c.** Cytofluorimeter PI staining to evaluate cell cycle in siCTRL and siCDH6 TPC1 and BCPap cell lines. **d.** Wound-healing assay to evaluate cell migration in siCTRL and siCDH6 TPC1 and BCPap cell lines. **e.** Matrigel-invasion chamber assay to evaluate cell invasion in siCTRL and siCDH6 BCPap cell line. N° of replicates =3 *P=0.05, **P=0.01, ***P=0.001.

ID	Frame	UniProtID	Length (aa)	N clones	CDS
GABARAP	1	Q6IAW1	117	5	complete
BNIP3L	1	Q6IBV1	219	2	complete
GATE16	1	P60520	117	1	complete
BNIP3	1	Q53HF4	194	1	complete

Figure 13. Most represented CDH6 interactors from the Membrane Yeast Two Hybrid assay.

GABARAP and GATE16/GABARAPL2 are ubiquitin-like proteins, part of the Microtubule-associated proteins 1A/1B light chain 3B (MAP1LC3B, LC3)/GABARAP protein family, orthologs of the yeast Autophagy Related 8 (ATG8) protein, and participate to the autophagosome formation the during the initial phases of autophagy (47).

BNIP3 and BNIP3L/Nix are implicated in apoptosis and mitophagy processes. BNIP3 binds and inhibits the anti-apoptotic Bcl2 proteins while it activates mitophagy through the interaction with LC3 and GABARAP (48).

CDH6 direct interaction with GABARAP, BNIP3 and BNIP3L was confirmed in vitro with a GST pulldown assay, while the interaction with GATE16 was not (Figure 14a).

Next, the significance of CDH6/GABARAP interaction in PTCs was investigated. First the effect of CDH6 silencing on autophagy activation was evaluated. To this end, the expression and localization of LC3 and GABARAP, markers of autophagy, was analyzed by western blot and immunofluorescent analysis (49). In the early phases of autophagy, LC3 and GABARAP are lipidated and loaded on autophagosome membrane to trigger its invagination. Later, after the fusion between autophagosome and lysosome, these proteins are degraded with the cargo.

In TPC1 cell line, western blot analysis showed that CDH6 silencing led to a significant endogenous LC3 and Flag-GABARAP down-regulation, suggesting autophagy induction (Figure 14b).

This hypothesis was investigated by chloroquine treatment and immunofluorescence staining. Chloroquine is a drug that interferes with the fusion between autophagosomes and lysosomes, thus impeding cargo degradation. Accumulation of LC3 following chloroquine treatment indicated that its degradation was due to autophagy activation enhancement and not to other biological processes (Figure 14c). Immunofluorescence staining for LC3 and GABARAP confirmed that upon CDH6 silencing autophagy is activated. These proteins, diffused in the cytoplasm in control cells, in silenced cells localized and co-localized into well-defined dots which are the newly formed autophagosomes (Figure 14d,e).

The PI3K-classI guides one of the most known anti-autophagic pathway and its inhibition, or the inhibition of its downstream targets like AKT and Mammalian Target Of Rapamycin Kinase (mTOR) provokes autophagy activation (50). Western blot analysis of the phosphorylated, active form of AKT showed that upon CDH6 silencing p-AKT is drastically down-regulated compared to control cells, in accordance with autophagy activation.

On contrast, the activation of the MAPK component Extracellular signal–Regulated Kinase (ERK) by AMP-activated Protein Kinase (AMPK) is reported to disassemble mTOR complexes 1 and 2 and enhance Beclin1-mediated autophagy (51). Thus, p-ERK levels were evaluated. p-ERK slightly increased upon CDH6 silencing, underling that other mechanisms were involved in the regulation of this process (Figure 14f).

All together, these data demonstrated that the binding of CDH6 and GABARAP is functional to control autophagy activation in thyroid cancer and that, when expressed, CDH6 restrains the activation of this process.
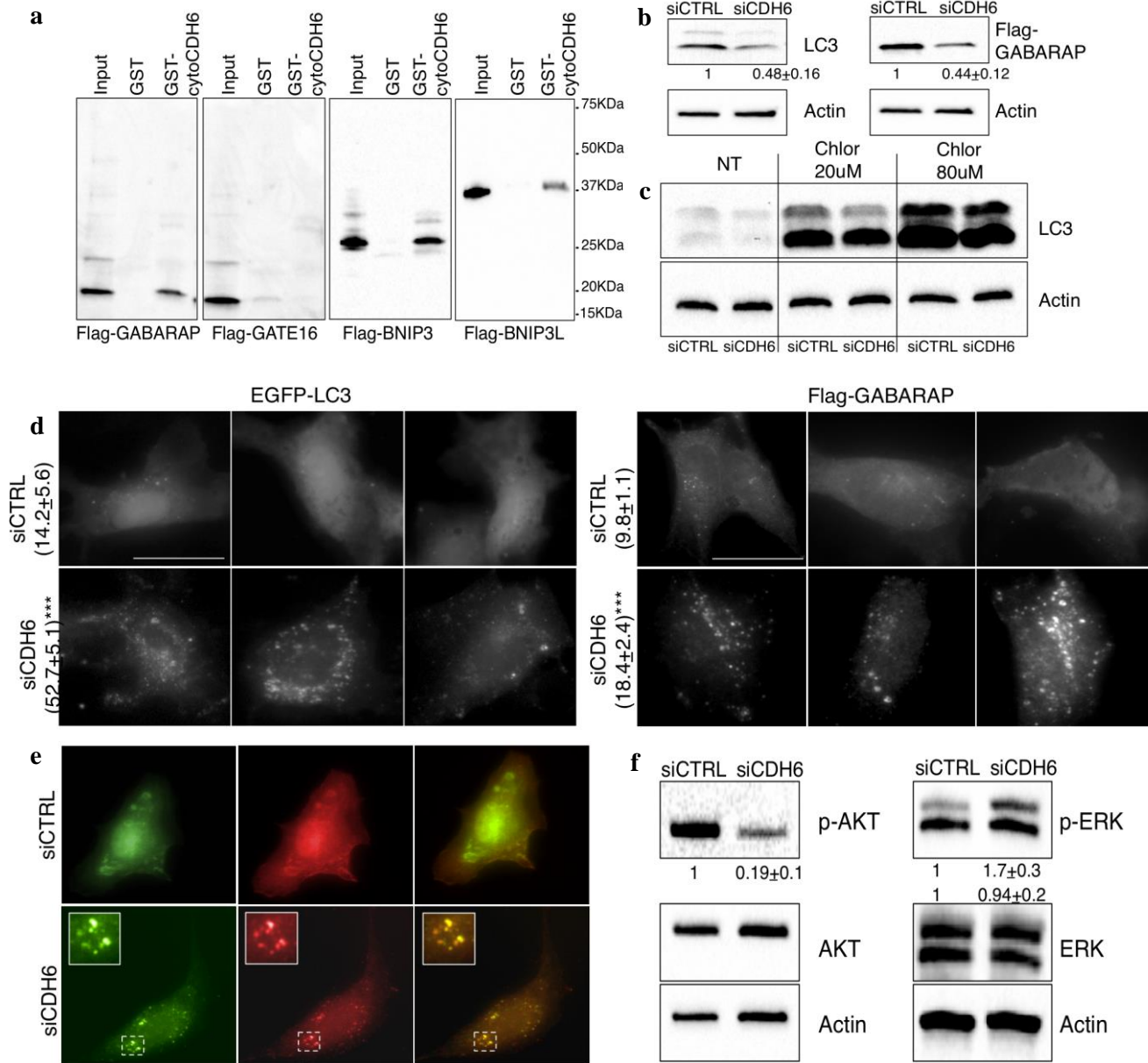
Figure 14. a. GST pull-down assay of cytoCDH6 with GABARAP, GATE16, BNIP3 and BNIP3L. Representative of four replicates. **b.** Western blot of endogenous LC3 and exogenous Flag-GABARAP in TPC1 cell line. The quantification refers to the percentage of LC3 and Flag-GABARAP normalized on actin levels in siCDH6 compared to siCTRL ±s.d. **c.** Western blot of LC3 in siCTRL and siCDH6 in not treated or chloroquine 20 or 80 µM treated TPC1. **d.** Immunofluorescence staining of EGFP-LC3 or Flag-GABARAP in siCTRL and siCDH6 TPC1. Quantification refers to the number of dots per cell ±s.e.m. **e.** Immunofluorescence showing the co-localization of EGFP-LC3 and Flag-GABARAP in siCTRL and siCDH6 TPC1 cells. **f.** Western blot analysis of pAKT, AKT, pERK and ERK in siCTRL and siCDH6 TPC1 cells. Quantification refers to the percentage of phosphorylated bands normalized on total protein levels in siCTRL compared to siCDH6 samples ±s.d. All the quantifications are calculated on the values obtained in three independent experiments ±s.d. N° of replicates =3   *P=0.05, **P=0.01, ***P=0.001.

CDH6 silencing affects mitochondrial dynamics and metabolism

The possible involvement of CDH6 in the regulation of mitochondria structure and function was also investigated. Mitochondrial network status following CDH6 silencing was assessed by mitotracker staining in TPC1 cell line. Immunofluorescence images showed a massive mitochondrial reorganization upon CDH6 silencing. In control cells, a hyper-fixed status was observed, while upon the silencing, massive mitochondrial fusion led to the establishment of a highly-interconnected network (Figure 15a,b). These morphological changes were accompanied by a strong down-regulation of exogenous BNIP3 and endogenous Dynamin-Related Protein1 (DRP1), the master regulator of mitochondrial fission (Figure 15c). Expression level of mitochondrial dynamics regulators was assessed by q-RT-PCR. Except for PINK1, no significant difference between control and CDH6-silenced cells was observed (Figure 15d). PINK1 was discovered in *Drosophila melanogaster* as a mitochondrial fission-promoting protein (52). Further studies on mammals revealed that its role is much more complicated and related to mitochondrial maintenance, biogenesis, transport and calcium homeostasis, and it is context dependent (53).

This observation indicates that CDH6 controls mitochondrial dynamics. Whether this effect is direct, or the consequence of autophagy activation remains to be determined.

Changes in mitochondrial morphology and shape not always reflects modifications of cell metabolism. However, inhibition of DRP1 has been shown to enhance mitochondrial fusion and promote oxidative phosphorylation (OXPHOS)-dependent ATP production, protecting mitochondria from degradation (54).

a siCTRL

b siCDH6

a1 a2 b1 b2

c

siCTRL siCDH6
Flag-BNIP3
1   0.48±0.16
Actin

siCTRL siCDH6
DRP1
1   0.61±0.12
Actin

d

■ siCTRL
■ siCDH6

TAZ DRP1 PINK1 OPA1 CRLS1 MFN1 FIS1 MFN2 CDH6

e

Lactate production

RLU

1500000

1000000

500000

0

BCPap siCT   BCPap siCDH6   Nthy-3.1-ori

f

350 Aerobic   Energetic

300

250

OCR (pmol/min)   200

◆ 150

100

50

0 Quiescent   Glycolytic

0   20   40   60   80   100   120

ECAR (mpH/min)

■ Nthy-ori-3,1   ■ BCPap siCT   ■ BCPap siCDH6

Figure 15. a,b. Immunofluorescence mitochondria staining with mitotracker red in siCTRL(**a,a1,a2**) and siCDH6 (**b,b1,b2**) TPC1 cell line. a1,a2,b1,b2 represent magnification of the upper images. **c.** Western blot analysis of exogenous BNIP3 and endogenous DRP1 in siCTRL and siCDH6 TPC1 cells. Quantification refers to the percentage of protein bands normalized on actin levels in siCDH6 compared to siCTRL ±s.d. quantifications are calculated on the values obtained in three independent experiments ±s.d. **d.** qRT-PCR analysis of relative expression of Tafazzin (TAZ), DRP1, PTEN-Induced putative Kinase 1 (PINK1), Mitochondrial Dynamin Like GTPase (OPA1), Cardiolipin Synthase 1 (CRLS1), Mitofusin 1 and 2 (MFN1-2), Fission 1 (FIS1) and CDH6 in siCDH6 and siCTRL TPC1 cells. **e.** Lactate production assay in BCPap siCTRL and siCDH6 and in Nthy-ori3,1 cells expressed in Relative Luminescence Units (RLU). Representative of three replicates. **f.** Energetic map of BCPap siCTRL, siCDH6 and in Nthy-ori3,1 cells. Representative of three replicates.

To assess if CDH6-mediated DRP1 modulation reflected a change in cell metabolism, Lactate production, Oxigen Consumption Rate (OCR) and Extracellular Acidification Rate (ECAR) were assessed in TPC1 cells treated with CDH6 siRNAs or scramble oligos and normal thyrocytes-derived Nthy-ori-3.1 cell line.

Since lactate is the main product of glycolysis, its measurement is a common and reproducible way to measure the glycolytic rate of a cell line in different conditions. Upon CDH6 silencing, lactate production diminished up to 50% in BCPap cell line reaching the levels measured in Nthy-ori-3,1 cells (Figure 15e).

To determine if the down-regulation of glycolysis following CDH6 silencing was due to a metabolism switch toward mitochondrial respiration, Seahorse assay was performed. OCR evaluates OXPHOS rate, while ECAR is a measure of the acidification of the cellular medium due to glycolysis-dependent protons extrusion. An energetic map was derived for Nthy-ori-3,1and for control or CDH6-silenced BCPap cells. While BCPap control cells showed a highly energetic profile, taking advantage of both glycolysis and OXPHOS, in accordance with their highly proliferative profile, CDH6-silenced cells displayed lower ECAR and OCR, according to their low proliferating

potential and quiescent state. Nthy-ori-3,1 as non-tumoral derived cell line whose metabolism relies mainly on OXPHOS, presented higher OCR and lower ECAR compared to BCPap cell line (Figure 15f). These results indicate that CDH6 not only affected mitochondrial morphology, but also participated to the regulation of cell metabolism. Since metastatic cancer cells that have undergone EMT are exposed to highly stressful condition, the ability of CDH6 to control cell metabolism unveiled a novel cadherin-mediated mechanism to sustain cancer metastasization.

CDH6 interaction with autophagic proteins is mediated by non-redundant LIR domains

The specific binding among autophagic machinery and other proteins involved in the process is usually mediated by the LC3-interacting region (LIR) motif. The LIR motif is constituted by a series of negatively charged residues followed by the sequence WxxL (55). In the cytoplasmic domain of CDH6 (cytoCDH6), 4 putative LIR motives (LIR 1-4) were found (Figure 16a). Deletion mutants for each LIR domain were obtained to assay by GST pull-down their role in the binding with CDH6 interactors. Absence of LIR2 completely abrogated the interaction between cytoCDH6 and GABARAP, while the binding between cytoCDH6 and BNIP3 and BNIP3L was mediated by LIR3. Interestingly, deletion of LIR3 also increased cytoCDH6 affinity for GABARAP, suggesting a structural impedance (Figure 16b).

These data indicated that multiple LIR domains were needed for CDH6 interaction with GABARAP, BNIP3 and BNIP3L/Nix and that these motives did not have a redundant role. Next, the possibility that other cadherins may play the same functions of CDH6 in other tissues was taken into consideration. The sequences of the members of the cadherin family were aligned. Intriguingly, 18
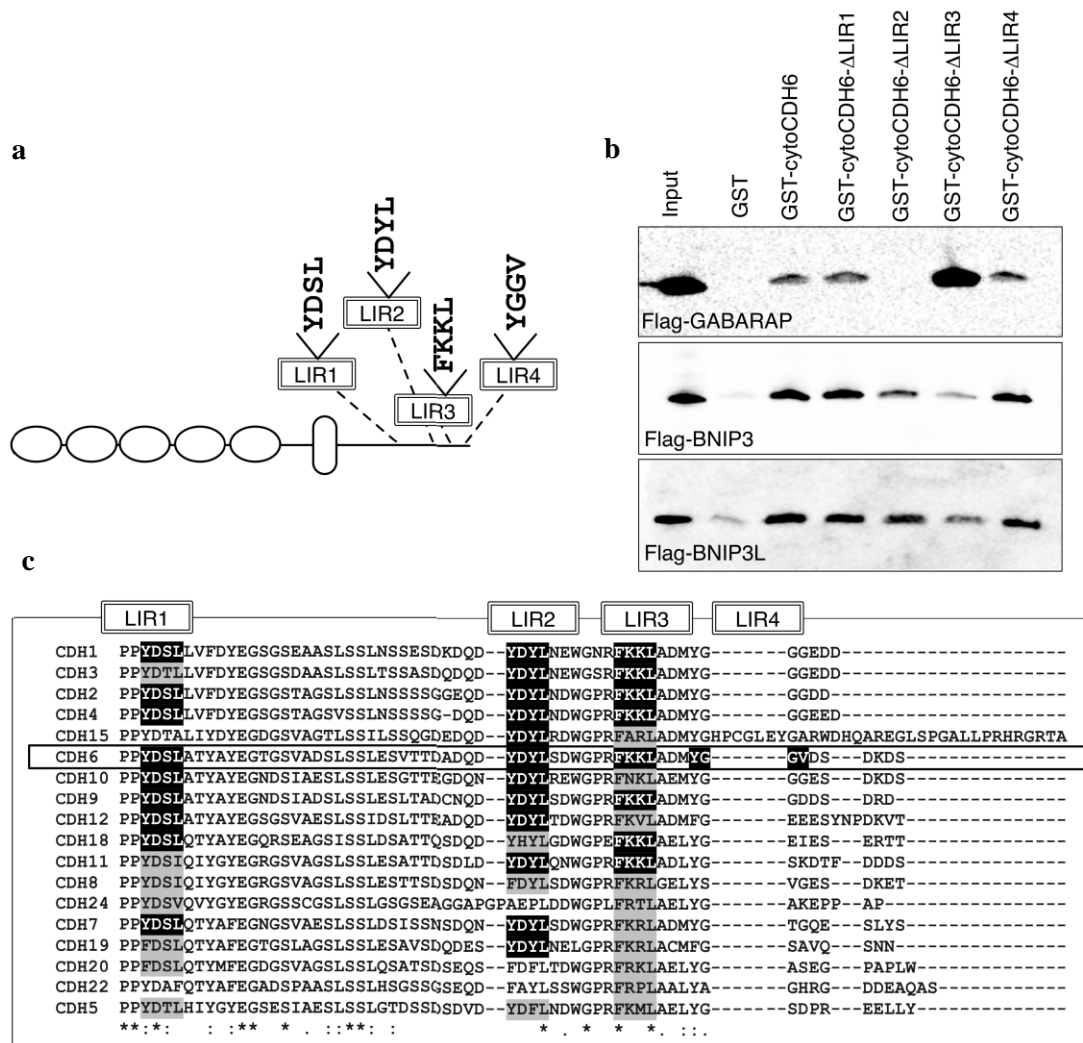
**Figure 16. a**. Illustrated representation of CDH6 structure highlighting the 4 LIR motives in the cytoplasmic domain and the respective aminoacidic sequence. **b.** GST pull-down of cytoCDH6 or its LIR deleted mutants with CDH6 interactors GABARAP, BNIP3 and BNIP3L/Nix. **c.** Alignment of cytoplasmic domains of cadherin family members highlighting the conservation of the four LIR domains found in cytoCDH6.

cadherins presented conserved LIR 1, 2 and 3 motives on their cytoplasmic domain, suggesting that other members of the cadherin family could interact with autophagic proteins and have a role controlling the process. In contrast, LIR 4 was only present in CDH6 sequence (Figure 16c). Remarkably, the epithelial CDH16, whose expression was enhanced in absence of CDH6, did not present any LIR motives, lacking the cytoplasmic domain. This observation suggested that switch between CDH16 and CDH6 in thyroid cancer functions as a crucial event in blocking autophagy, promoting the acquisition of an EMT phenotype in this tumor.

CDH6 membrane localization is needed for its function

To try to revert the phenotype observed upon silencing experiments previously performed, CDH6 over-expression in TPC1 cell line was carried out. Since it was not possible to over-express the full-length protein, only the cytoplasmic domain of CDH6, which contains LIR motives and can interact with BNIP3, BNIP3L and GABARAP was used. The effects of the transfection of cytoCDH6 were assessed by western blot to check the levels of the key protein found altered in the CDH6-silencing experiments. cytoCDH6 overexpression did not alter the control cells phenotype (Figure 17). This result may imply that the whole CDH6, and particularly its transmembrane domain which allows its localization on the plasma membrane, is necessary to induce cytoskeleton reorganization and to restrain autophagy.
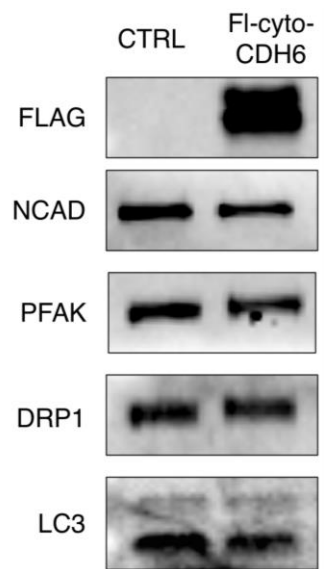
Figure 17. Western Blot analysis of N-CAD, pFAK, DRP1 and LC3 in control or transfected with Flag-cytoCDH6 TPC1 cells.

*Genome-wide analysis of H3K27AC profile during TGFβ -mediated EMT*

The recent systematic functional analysis of noncoding genome by the ENCODE project has revealed that gene expression is far more complicated than expected and that the precise spatiotemporal expression of a gene needs a continuous and widespread regulatory landscape involving a specific genomic architecture and the hierarchical interactions of multiple interspersed regulatory elements (56). Furthermore, the ENCODE project demonstrated that chromatin exists in multiple functional states, which correlate with the extent of gene expression. This implies the possibility to predict gene expression variations by picturing the overall landscape of chromatin functional status. TGFβ-mediated EMT is sustained by the activation of a complex transcriptional program. However, the genome-wide effect of TGFβ on the transcriptional activation status of the chromatin has not yet been described. Furthermore, it was demonstrated that also CDH6 expression is controlled at the transcriptional level by TGFβ during EMT and that the transcription factor RUNX2 partially mediates this activation, even though the exact mechanism of this regulation is still to be defined. Acetylation of lysine 27 of histone 3 (H3K27ac) is commonly used to map transcriptionally active regulatory elements (57,58).

In the attempt to mark TGFβ responding transcriptional elements adding information on the regulatory network during EMT, and to find CDH6 regulatory regions, analysis of genome-wide changes in the profile of H3K27ac upon TGFβ stimulation was performed.

Chromatin Immuno-Precipitation followed by sequencing (ChIP-seq) analysis for H3K27ac on Nthy-ori-3,1 cells treated with TGFβ or not treated was performed. 22775 peaks were called in this analysis. Peak to target assignment was used to associate each detected peak with the nearest Transcription Starting Site (TSS). The distribution of the peak distances to the nearest TSS is displayed in Figure 18a.

Figure 18b shows the Venn Diagram representing the total number of TSS-associated regions that were defined by this analysis. 8604 TSS-associated regions presented the same peaks in both experimental conditions, 48 had enriched peaks only in condition 1 (NT) and 1025 had enriched peaks only in condition 2 (TGFβ). Of these, 164 regions were specific of one condition, 10 were exclusive of NT cells while 154 were detected solely in TGFβ-treated condition (Figure 18c). Alignment of the detected peaks to the human reference genome (GRCh38/hg38) showed no peaks in either condition (NT or TGFβ) within the CDH6 locus (Figure 19a). This could be determined either by the fact that the TGFβ effect on CDH6 is not mediated by changes in the chromatin transcriptional status of the gene locus, or by the fact that some regions were not correctly covered by the sequencing. However, also the analysis of the ENCODE annotation data for the CDH6 locus, in non-thyroid derived cell lines, did not evidenced any relevant H3K27ac peak.

By contrast, analysis of well-known TGFβ target genes, like N-CAD and SNAI1, showed a significant peak enrichment in TGFβ-treated cells (Figure 19b,c) coherently with the gene expression induction of these transcripts (Figure 19d).
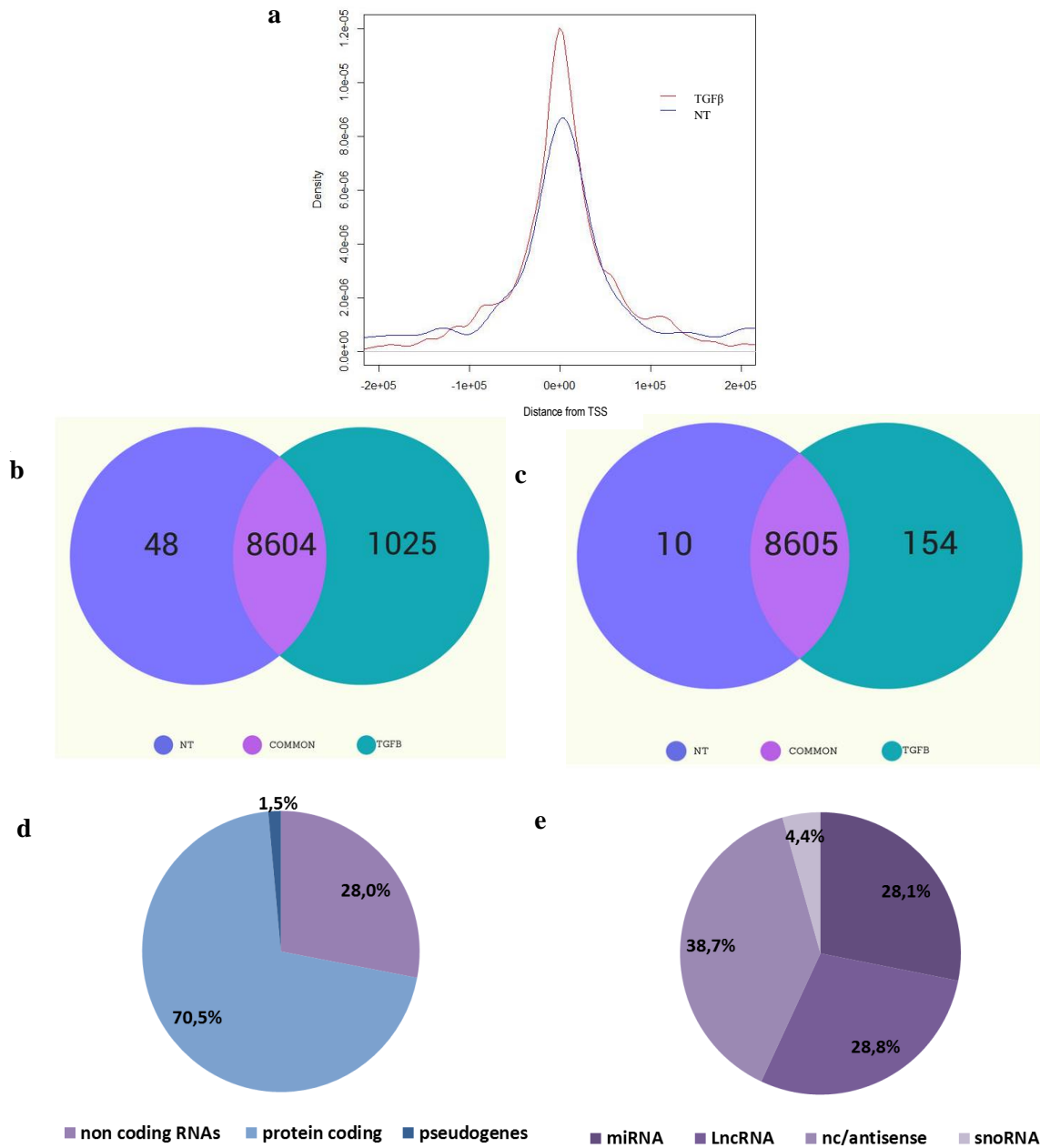
Figure 18. a. Density vs distance from Transcription Starting Site (TSS) of the peaks called in the ChIP-seq analysis for the two conditions (NT and TGFβ). **b.** Venn diagram showing all genes correlated to enriched H3K27ac peaks resulted from ChIP-seq analysis in not treated, TGFβ treated or in both conditions. **c.** Venn diagram showing genes correlated to enriched H3K27ac peaks from ChIP-seq analysis only present in NT or TGFβ condition. **d.** Pie chart representing the different typologies of transcripts distribution among the TSS-associated regions enriched in TGFβ condition. **e.** Pie chart displaying the distribution of non-coding RNAs typologies among the non-coding TSS-associated regions enriched in TGFβ condition.
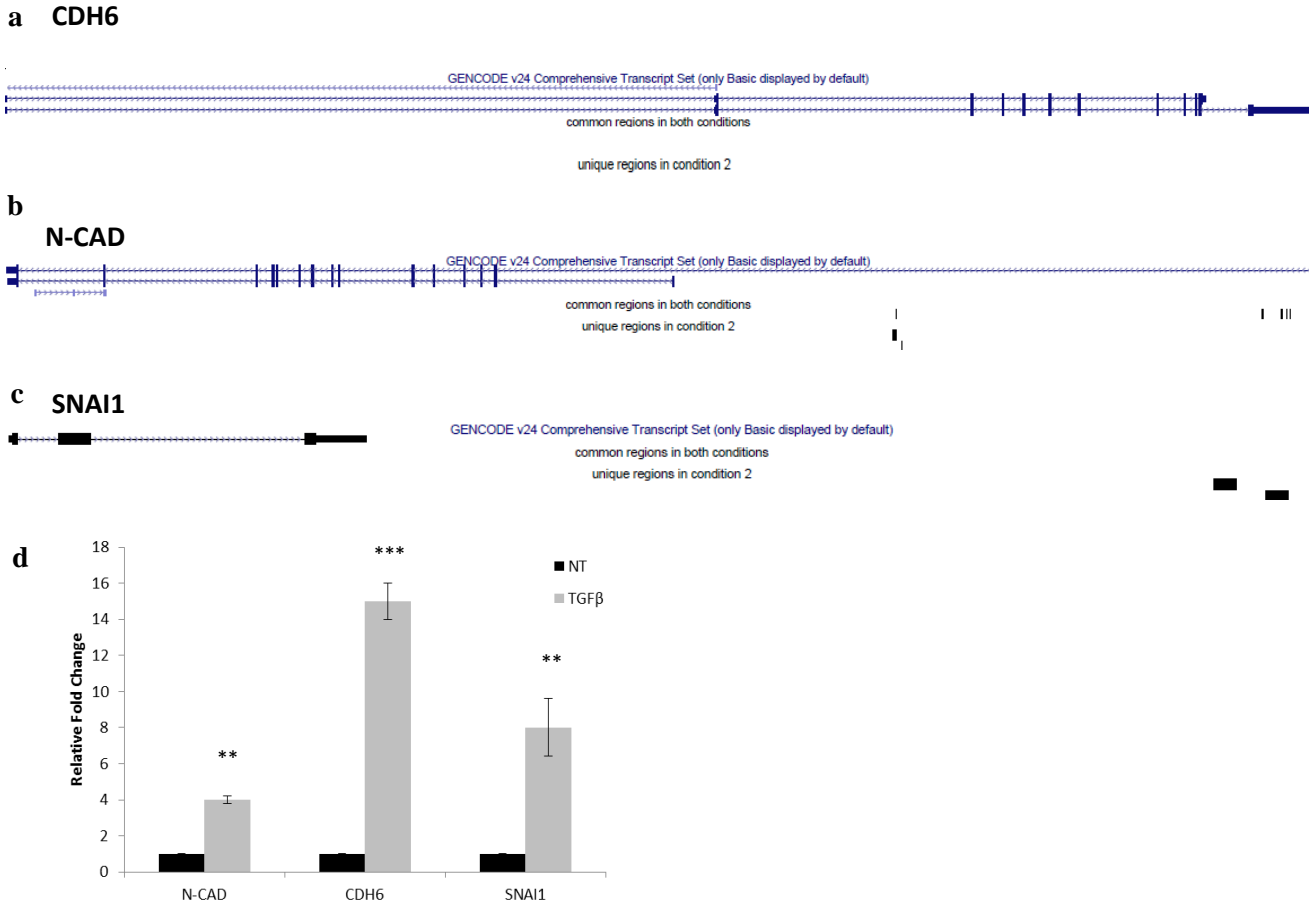
Figure 19. a-c. Evaluation of H3K27ac peaks enrichment in CDH6 (**a**), N-CAD (**b**) and SNAI1 (**c**) loci. Peaks found in both conditions (NT and TGFβ treated), or unique regions found in condition 2 (TGFβ) are shown. **d.** Relative expression of N-CAD, CDH6 and SNAI1 in Nthy-ori-3,1 not treated or treated with 5 or 100 ng/ml of TGFβ. N° of replicates =3 *P=0.05, **P=0.01, ***P=0.001.

Next, we focused on the 1025 TSS-associated regions detected upon TGFβ treatment.

Among these, 70,5% (723/1025) were protein-coding genes, 28% (287/1025) were regions transcribing for non-coding RNAs and 1,5% (15/1025) were pseudogenes (Figure 18d). Among the non-coding elements, 38,7% (106/287) were non-coding or antisense RNAs, 28,8% (79/287) were long non-coding RNAs (LncRNAs), 28,1% (77/287) were micro RNAs (miRNAs) and 4,4% (12/287) were small-nucleolar RNAs (snoRNAs) (Figure 18e). These results were very interesting

since nc-RNAs control gene expression from transcription to protein stability, localization and function (59). Indeed, the role of non-coding RNAs as regulatory molecules and key regulators in physiological and pathological contexts is opening new perspective in this field of study (60).

Afterwards, Gene Ontology enrichment analysis was performed to define pathways significantly affected by TGFβ signaling in thyroid cells (Table 6).

TABLE 6 Gene Ontology analysis

Pathway ID	Pathway description	Gene count	False discovery rate
GO.0009653	anatomical structure morphogenesis	150	4.16e-18
GO.0009966	regulation of signal transduction	146	1.08e-11
GO.0048869	cellular developmental process	181	1.08e-11
GO.0048518	positive regulation of biological process	245	1.26e-11
GO.0030154	cell differentiation	173	2.25e-11
GO.0048646	anatomical structure formation involved in morphogenesis	80	6.16e-11
GO.0009893	positive regulation of metabolic process	186	6.65e-11
GO.0007165	signal transduction	227	1.19e-10
GO.0044700	single organism signaling	238	1.19e-10
GO.0007154	cell communication	241	1.83e-10
GO.0010646	regulation of cell communication	159	1.83e-10
GO.0023051	regulation of signaling	153	1.97e-10
GO.0048731	system development	186	2.18e-10
GO.0048856	anatomical structure development	206	3.6e-10
GO.0048519	negative regulation of biological process	209	7.68e-10
GO.0048522	positive regulation of cellular process	212	1.29e-09
GO.0050793	regulation of developmental process	124	2.39e-09
GO.0048523	negative regulation of cellular process	195	3.16e-09
GO.0051716	cellular response to stimulus	265	3.39e-09
GO.0007399	nervous system development	119	3.47e-09
GO.0032502	developmental process	221	4.76e-09
GO.0051128	regulation of cellular component organization	124	1.07e-08
GO.0051270	regulation of cellular component movement	59	2.56e-08
GO.1902531	regulation of intracellular signal transduction	90	3.06e-08
GO.0040011	locomotion	81	3.54e-08
GO.0022008	neurogenesis	90	5.14e-08
GO.0030198	extracellular matrix organization	38	8.94e-08
GO.0031325	positive regulation of cellular metabolic process	147	8.94e-08
GO.0048729	tissue morphogenesis	50	1.16e-07
GO.0030334	regulation of cell migration	51	1.46e-07
GO.0042060	wound healing	55	1.9e-07
GO.2000145	regulation of cell motility	52	3.61e-07
GO.0040012	regulation of locomotion	54	6.57e-07
GO.0006950	response to stress	161	6.07e-06
GO.0006935	chemotaxis	48	6.29e-06
GO.0007155	cell adhesion	63	1.02e-05
GO.0016477	cell migration	52	2.55e-05
GO.0008284	positive regulation of cell proliferation	54	3.08e-05
GO.0090287	regulation of cellular response to growth factor stimulus	25	3.64e-05
GO.0000902	cell morphogenesis	60	3.84e-05
GO.0030155	regulation of cell adhesion	43	3.84e-05
GO.0030029	actin filament-based process	35	4.52e-05
GO.0032270	positive regulation of cellular protein metabolic process	75	4.54e-05
GO.0030036	actin cytoskeleton organization	33	4.97e-05
GO.0042221	response to chemical	167	5.19e-05
GO.0019222	regulation of metabolic process	254	6.03e-05
GO.0051674	localization of cell	54	6.09e-05
GO.0048870	cell motility	54	6.3e-05

Furthermore, protein-protein network analysis was performed using STRING database. Several gene modules were predicted from this analysis (Figure 20). Among the discovered modules, in accordance with the pathways found in the GO analysis, proteins involved in structure, morphogenesis and cell motility were found. This is in line with the fact that TGFβ-mediated EMT massively relies on the re-organization of cell structure and on the reactivation of morphology-related genes (Figure 20a). These modifications also involve the up-regulation of genes which promote cell motility, to sustain cell migration (Figure 20b). Noticeably, several genes networks were detected, including endocytosis related genes and components of the PI3K–pathway respectively (Figure 20c,d). This further underlines the involvement of autophagy in TGFβ-mediated EMT and supports our data.

In conclusion, these data are in accordance with the role of TGFβ in mediating EMT also in thyroid cancer cells, but, most importantly, sustain the hypothesis that EMT activation in these cells is related to a massive re-organization of the transcriptional program which involves pathways that regulate autophagy and cell metabolism.
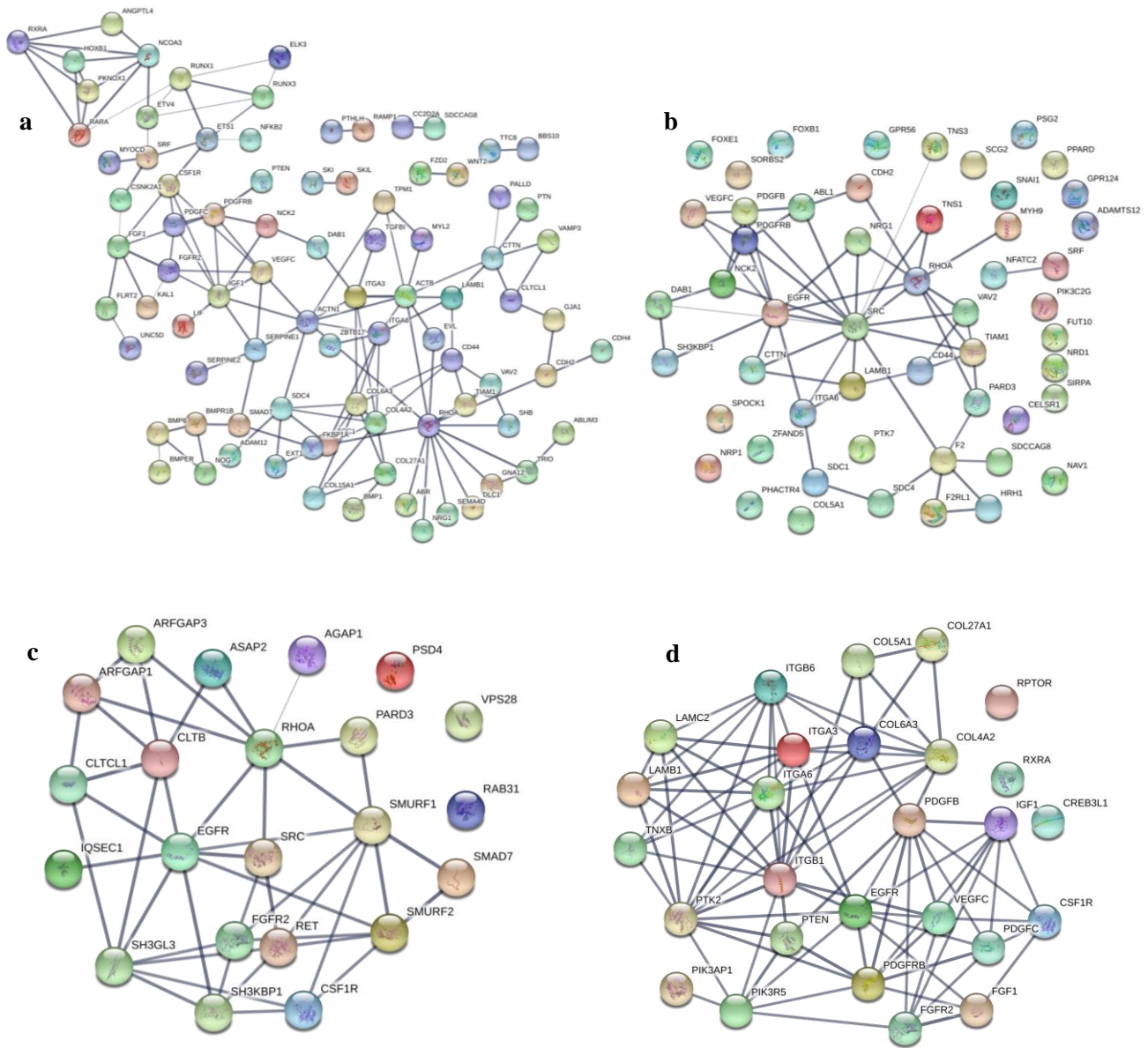
Figure 20. Examples of STRING protein-protein interaction prediction of the genes enriched in TGFβ-treated cells, based on ChIP-seq data. **a.** Anatomical structure morphogenesis. **b.** Cell migration. **c.** Endocytosis

Discussion

Cadherins are transmembrane proteins which major function is to organize cell-cell and cell-microenvironment interactions. However, cadherins are not just structural proteins, but they also act like hubs for the intracellular signaling transduction controlling many cellular processes. The way cadherins mediate biological processes, including transcriptional regulatory pathways, still needs to be characterized.

In this study, we showed for the first time that CDH6 supports EMT and interferes with autophagy and mitochondrial dynamics, highlighting a previously unknown function of cadherins in cancer.

Based on our data, we proposed the following model: CDH6 expression is up-regulated following pro-metastatic signals like TGFβ. CDH6 substitutes epithelial cadherins like CDH16 on cell membrane, leading to changes in cytoskeleton architecture and loosening of cell-cell interactions, promoting cell migration and invasiveness. CDH6 direct interaction with GABARAP restrains autophagy, overcoming the negative effect of this process on EMT completion. Finally, CDH6-mediated autophagy repression promotes DRP1-mediated mitochondrial hyper-fission, which in turn provides faster ATP production necessary for cytoskeleton rearrangement and for the development of movement structures (Figure 21). Finally, we proved that CDH6 expression is a highly specific marker of metastatic well-differentiated PTCs, laying the basis for its possible use for risk-based stratification in the clinical setting of thyroid cancer patients.

We demonstrated that autophagy activation is regulated by CDH6 direct interaction with GABARAP but the process is also affected by the regulation of the activation state of the autophagy-modulator protein AKT. Thus, we hypothesize that CDH6 restrains autophagy both directly, binding GABARAP, and indirectly, through a signal transduction regulation which affects the activation of the PI3K-classI pathway. In accordance with our hypothesis, a recent work showed that GABARAP

expression negatively correlates with AKT phosphorylation inhibiting prostate cancer proliferation and metastasization (61).

EMT and autophagy are biological processes with a pivotal role in cancer development and progression. The catabolic function of autophagy aids cancer cells to overcome the great variety of stresses to which they are exposed during tumor progression, including deprivation of oxygen and nutrients. On the other side, EMT transdifferentiation allows cancer cells to acquire mesenchymal features that support cell proliferation and migration (18).

Recently, several studies addressed the complex relationship between EMT and autophagy, demonstrating that the interplay between these processes in cancer is tissue and phase-dependent.

On one hand, cells in which the EMT program is activated require autophagy to survive during the metastatic spreading. On the other hand, during the early phases of cancer metastasization, autophagy acts as oncosuppressive process degrading crucial EMT-driving transcription factors (62-64).

To date, the molecular mechanisms that regulate the interplay between autophagy and EMT is far to be fully characterized. However, several observations suggest that the functional interaction between cytoskeleton and mitochondria is a regulatory center connecting these two processes (65,66).

Cytoskeleton controls mitochondrial dynamics, cooperating to dictate mitochondria availability along the cell. This process controls the number and structure of mitochondria, regulating cancer cells energy production, which in turn is necessary to re-organize cytoskeleton and to sustain EMT-induced cell movement (18). Our data is in agreement with this model, indeed, CDH6 silencing can partially revert EMT program, changing cytoskeleton organization and modifying both mitochondrial structure and function (Figure 21).

Differently from what usually assumed, EMT is not a single-step process but cancer cells must undergo through series of progressive stages to fully accomplish this transdifferentiation. Recently,

Klymkowsky and Savagner debated about the erroneous use of the general term EMT to describe all these intermediate stages, clarifying that it would be more appropriate to talk of EMT-related processes (67).

We showed that CDH6 positive cells, localized at the invading front of the tumor mass, still retained E-CAD expression. This suggests that these cells reside in a partial EMT state, recalling of a phenomenon called collective cell migration.

During collective cell migration, cells undergo a partial EMT, changing their morphology toward a spindle like phenotype and re-organizing cell cytoskeleton and cell-cell adhesions (68). In these invading cells, E-CAD expression is an advantage to maintain cell cohesiveness, that in turn facilitate migration, protecting single cells from external mechanical stresses (69). Several studies, indeed, demonstrated that collective cell migration is the main modality of tumor cells invasiveness and significantly contributes to epithelial cancer metastatic spreading (70,71).

Autophagy activation may affect mitochondrial dynamics in two opposite ways. On one side, autophagy as catabolic process can target mitochondria to degrade them. This process, called mitophagy, requires mitochondrial fission in order to allow autophagosomes to engulf and degrade single mitochondria. On the other side, the massive activation of autophagy has been reported to promote mitochondrial fusion to protect these organelles from massive degradation. Noticeably, the autophagy-related mitochondria hyper-fusion has been associated with cell migration inhibition (72,73).

The complex interplay between autophagy and mitochondrial dynamics is crucial to determine cell fate and behavior, and cytoskeleton is a fundamental player in this crosstalk. Indeed, cytoskeleton acts like a mechanical regulator of mitochondrial morphology and localization. Whether these changes also reflect a modification in mitochondrial function is still to be defined. Unbalance

between mitochondrial fusion and fission could modify mitochondrial localization thus interfering with some cellular functions that require a specific location of these organelles (74).

In this work, we described for the first time BNIP3 and BNIP3L/Nix, mitochondria-associated proteins as novel CDH6 interactors. BNIP3 was observed to support cell migration by remodeling cell-cell interaction and cytoskeleton in a melanoma cell line. Surprisingly, the downregulation of BNIP3 expression led to a phenotype which resembles the one we observed after CDH6 silencing in thyroid cancer cell lines (75). BNIP3L/Nix was recently discovered to regulate cell differentiation through cell metabolism reprogramming. Up-regulation of BNIP3L/Nix following hypoxia stimulates mitophagy activation, promoting glycolytic metabolism (76).

Furthermore, CDH6 induces DRP1-mediated mitochondrial fission, providing a large number of single-unit mitochondria needed for the energetic requirement of the cell (Figure 21). DRP1 is the master regulator of mitochondrial fission, described as a relevant promoter of cell migration and aggressiveness in different types of tumors (e.g brain, breast, lung). Its upregulation, and the subsequent mitochondrial hyper-fission are features of metastasization and poor outcome, in turn, targeting its expression leads to apoptosis and diminished tumor growth (77-79). Indeed, several studies showed that DRP1 expression is higher in metastatic cancer cells than in non-metastatic ones (80). This evidence further supports our data and our model.

The observations of Otto Warburg, dating back 100 years, that cancer cells have a different metabolism compared to normal somatic cells and are able to exploit glycolysis, producing energy at higher speed also in presence of oxygen, opened a new field of study (81). Currently, claiming that tumor cells simply switch their metabolism from OXPHOS to an accelerated glutaminolysis and aerobic glycolysis is an over-simplification (82). It is now established that cancer cellular metabolism depends on many variables, among which "alternative" energetic sources including metabolites from

the microenvironmental stroma, that may contribute to rewire and support cancer energetic production (83). It is not surprising that aggressive cells undergoing an EMT program, which are prone to leave primary sites to colonize other tissues, need a highly energetic metabolism which is sustained both by aerobic glycolysis and oxidative phosphorylation. Considering the importance of this topic, the role of oxidative phosphorylation and mitochondria in cancer is gaining increasing attention and a strong debate on whether mitochondrial morphology affects their functionality in cancer is open.

Although preliminary, our data indicate that CDH6 not only influences the morphology of the mitochondrial network, but also changes the way thyroid tumor cells produce the energy necessary for proliferation and migration. We demonstrated that the expression of CDH6 is correlated with a highly energetic metabolism, which likely allows cells to undergo dynamic changes and metastasization. On contrast, cells in which CDH6 expression was down-regulated were more quiescent and presented energetic profiles more similar to normal thyrocytes-derived cells.

The abundance of spared mitochondria, derived from DRP1-mediated fission, allows cells to maintain high energy production levels, and to re-locate free mitochondria across the cytoplasm to the cell districts where they are more needed in a precise moment. At the same time, in accordance with their need for more energy, cells start to take advantage also of glycolysis for ATP production.

The statement that cancer cells are not able to exploit mitochondrial respiration is untrue, indeed recent works showed that increased oxidative phosphorylation supports cell proliferation and metastasization capacity and it associates with tumor suppressor loss (84).
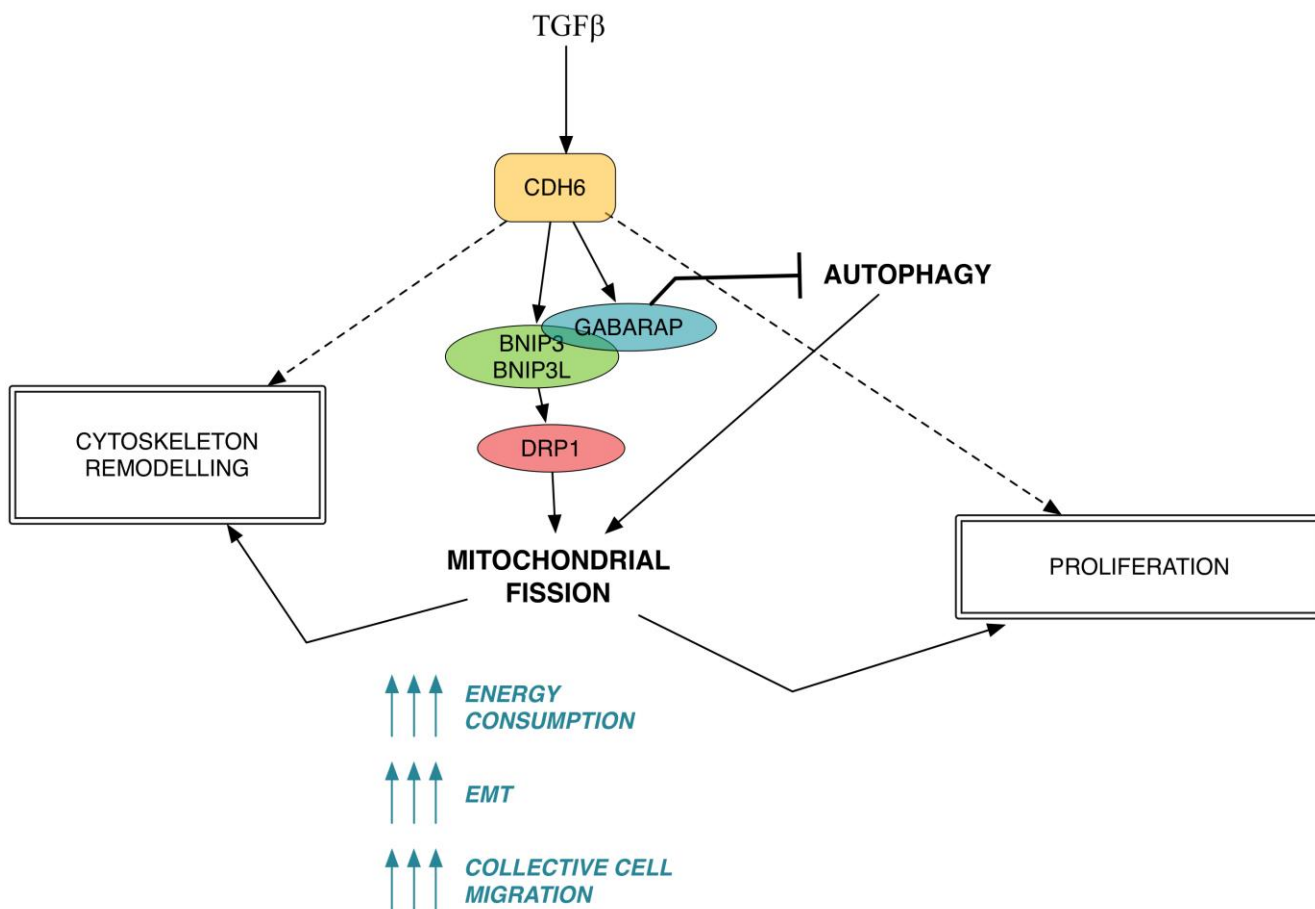
Figure 21. Model of CDH6 function in thyroid cancer cells.

TGFβ signaling in thyroid cancer

The transcriptional program mediated by TGFβ in thyroid cells is still to be characterized, and would help to understand the molecular mechanisms at the basis of TGFβ-mediated transdifferentiation and to develop systems to counteract its accomplishment.

Our ChIP-seq analysis aimed to study the regulatory network during EMT, and to find CDH6 regulatory regions which guide its re-expression in thyroid cancer cell. Focusing on the TSS-associated regions detected upon TGFβ treatment, we showed that TGFβ changes the distribution of

the open-chromatin marker H3K27ac across the genome, increasing its accumulation in regions related to genes known to be involved in TGFβ signaling.

Non-coding RNAs control gene expression from transcription to protein stability, localization and function. A fraction of these, the long non-coding RNAs (lnc-RNAs) are longer than 200 nucleotides and share similarities to protein-coding genes, being transcribed by RNA polymerase II and displaying intron-exon organization (85). Unbiased genome-wide searches discovered thousands of lncRNAs and their total number is currently estimated to triple the number of protein coding genes. Based on their large number and expression specificity, lnc-RNAs are expected to contribute to many cellular processes, including oncogenic signaling (86). More than 8,000 lnc-RNA were recently discovered to be highly specific in cancer, representing a potential tumor-specific reservoir for biomarkers and therapeutic targets (87). Not surprisingly, among the TGFβ-regulated TSS-associated regions detected in our analysis we found a large amount of regions transcribing for non-coding RNAs. Currently, the function of only few lnc-RNAs has been characterized. Thus, we aim at extending this observations, to get a deeper knowledge on the role of lncRNAs in mediating TGFβ signaling in cancer.

Unfortunately, the ChIP-seq approach failed to identify potential TGFβ responsive elements within the CDH6 locus. This could be determined by the fact that the TGFβ –dependent CDH6 induction is not regulated at the transcriptional level, even though we already demonstrated in previous works that TGFβ-mediated CDH6 induction requires the transcription factor RUNX2. On the other hand, technical problems could have impaired the analysis within this locus, since in normal thyrocytes-derived cell lines CDH6 expression is very low, suggesting that the gene locus is in a heterochromatin region. Indeed, chromatin structure and accessibility is one of the main biases when performing ChIP and ChIP-seq analysis. Indeed, open-chromatin regions seem to be preferentially

represented after the fragmentation steps, and could cause false-positive enrichment peaks. In contrast, heterochromatin regions are more difficult to shear and could result in an underestimation of the enrichment peaks (88).

Overall, our data describe:

- New insights into the molecular mechanisms regulating thyroid cancer progression.

- New functions for cadherins in the regulation of autophagy and mitochondrial dynamics.

- New mechanisms regulating the interplay between EMT and autophagy in cancer.

Moreover, this work opens new frontiers in the discovery of coding and non-coding transcripts which mediate TGFβ signaling in thyroid cancer cells.

Furthermore, CDH6, for its potential role in mediating thyroid cancer cells aggressiveness, could be proposed as a new prognostic marker for patients risk-based stratification, and as a new target for anticancer therapy. Indeed, a recent work tried to develop antibody-drug conjugates to guide cytotoxic agents preferentially to the sites of the tumor. CDH6 was selected as a target as its expression is strictly regulated and tissue-specific. The study was performed in ovarian and renal cancers, in which CDH6 is over-expressed, with good results. Thyroid cancer could be proposed as another target for this promising study (89).

<u>Materials and Methods</u>

Cell cultures

Papillary Thyroid Carcinoma BCPap and TPC1 and Normal Thyrocytes-derived Nthy-ori 3-1 cell lines were obtained from Dr. Massimo Santoro, University of Naples.

All cell lines were grown at 37°C and 5% CO_2, BCPap and TPC1 in DMEM and Nthy-ori 3-1 in RPMI supplemented with 10% fetal bovine serum, 2 mM of glutamine and antibiotics (penicillin, 100 U/ml and streptomycin, 100 μg/ml). All cell lines were authenticated at Multiplexion GmbH by Single Nucleotide Polymorphisms genotyping.

Cell transfection

For RNA Interference transfection, Stealth siRNA oligos targeting CDH6 and scramble oligos as negative control were purchased by Thermo Fisher Scientific (Monza, Italy). 20 nM oligos were transfected following a reverse transfection protocol using RNAiMax Lipofectamine (Thermo Fisher Scientific, Monza, Italy) in a 6 well plate or 10cm dish. 32 hours after transfection cells were harvested and seeded in 24 wells or slide chambers for Immunofluorescence analysis to maintain the same cell density, and the analysis were performed after 12 hours. The timing for all the functional analysis was the same with the exception of the cell morphology analysis, which was performed 96 hours after siRNA transfection. For plasmid transfection, Lipofectamine 2000 (Thermo Fisher Scientific, Monza, Italy) was used. For siRNA and plasmid co-transfection, 48 hours after siCDH6 or scramble oligos transfection with RNAiMax Lipofectamine, cells were seeded and transfected with the selected plasmid using Lipofectamine 2000 and after 24 hours cells were analyzed. siCDH6 efficiency is reported in Figure 9a-c.

Patients selection

The Pathology Unit of Azienda USL of Reggio Emilia archive counts over 2900 thyroid cancer samples, collected in over 30 years. Among these, we retrieved 86 well-differentiated PTCs. Screening and classification of tumor slides were performed by pathologists according to the World Health Organization Classification of Tumors, to exclude high-grade carcinomas, and to the American Joint Committee on Cancer Staging Manual (7th edition). Based on a 7 years follow-up, 44 PTCs that developed distant metastases (DM-PTCs) and 42 controls that did not (nM-PTCs), matched by age, were identified. Among the DM-PTCs, 36% presented distant metastases at the time of diagnosis (synchronous) while in 64% metastases arose later (metachronous). All the patients underwent thyroidectomy, and on the 80% of them were also performed ipsilateral central neck dissection.

Immunohistochemistry

4 μm FFPE (formalin fixed paraffin embedded) histological sections were stained with anti-CDH6 antibody (HPA007047, Sigma Aldrich, Milan, Italy), and anti-ECAD antibody (clone 36, 790-4497, Ventana-Roche) and counterstained with hematoxylin. For TPC1, BCPap and MCF7 (negative control) cell lines Immunohistochemistry, $2*10^6$ cells were harvested, 4% formalin fixed (10 minutes), centrifugated and resuspended in 0.8% agar (in PBS 1X) for paraffin inclusion. 5 μm sections were stained with the same protocol used for tissue samples. Specificity control for the stain is showed in (Figure 22). Nikon Eclipse E80 microscope was used to capture IHC images. The project was approved by the Azienda USL – Reggio Emilia ethics committee and informed consent was obtained from all the patients.
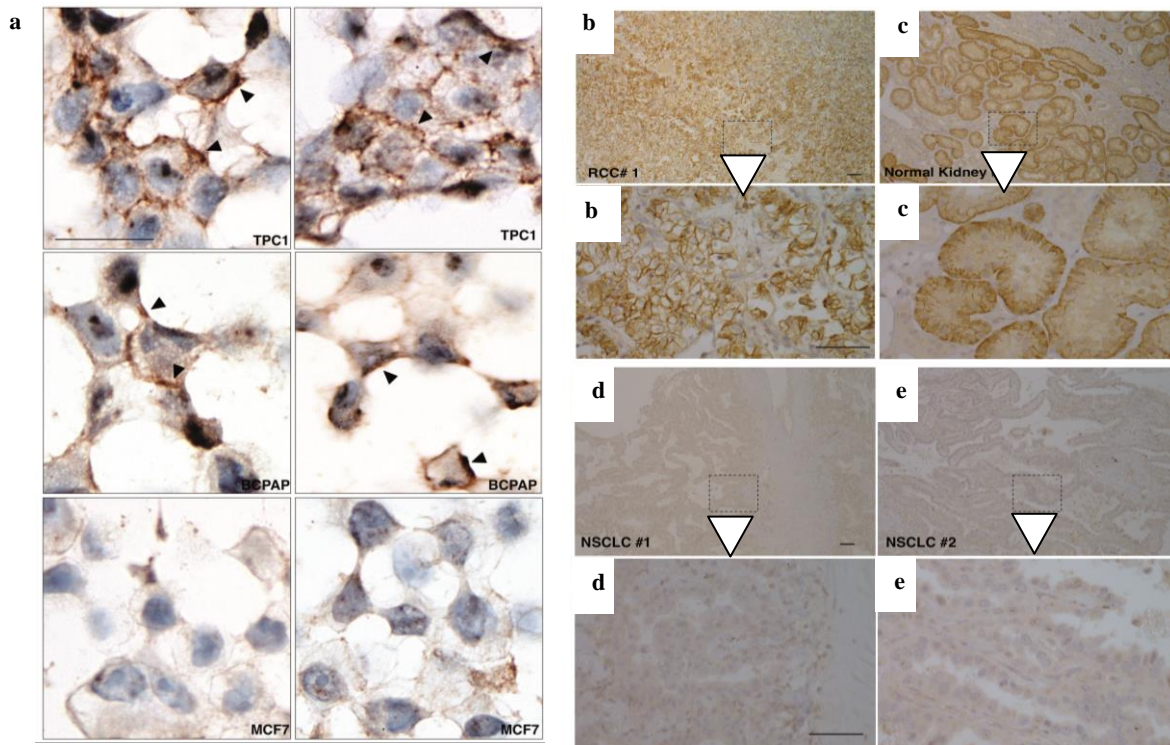
Figure 22. IHC. Specificity of the anti-CDH6 antibody on TPC1, BCPap and MCF7(negative control) cell lines (**a**) and on renal cell carcinoma (RCC)(**b**), normal kidney (**c**) and non-small cell lung cancer (NSCLC) (negative control) (**d,e**) tissues. Black arrows indicate CDH6 staining on the cell membrane. White arrows represent higher magnification of the selected areas.

Membrane Yeast Two Hybrid screening

Membrane Yeast Two Hybrid screening was performed by DualSystems Biotech AG (Switzerland), taking advantage of the split-ubiquitin system designed for membrane proteins. CDH6 (bait protein) was fused to the C-terminal half of ubiquitin (Cub) and to a transcription factor while the pray protein library was fused to the N-terminal half of ubiquitin (Nub). If the association between the bait and the prey occurs, a compete ubiquitin molecule is recomposed, the transcription factor is cleaved from the bait by endogenous protease, leading to its release and to the expression of the reporter genes in yeast

genome. The bait was made using the full-length cDNA encoding human CDH6 cloned in pBT3-SUC vector, while the prey library was obtained by 5 PTC samples selected from the Head and Neck Tumors Biobank of our institution. Total RNA was extracted and pooled to obtain a cDNA library cloned in the pPR3-N vector. The library was normalized removing high abundant transcripts to ensure good representation of low abundant ones and to reduce false positives. $2.8 * 10^6$ independent clones with average size of 1.5 kb were obtained. Bait and cDNA library were transfected into NMY32 yeast host strain. $3.8 * 10^6$ transformants were screened and 39 positive clones were found. The identity of positive interactors was defined by sequencing the library plasmids isolated from positive clones and searching the sequences against the Swissprot database, using BLASTX algorithm.

GST Pull-Down

The sequence of the cytoplasmic domain of CDH6, or the sequences mutated for LIR domains 1-4 were cloned into the pGEX-6P-1 plasmid within SmaI and XhoI sites, in frame with N-terminal GST. E.Coli BL21 were transformed with the plasmids and grown overnight. After 12 hours the cultures were diluted 1:100 in 50 ml of LB supplemented with 100 mg/ml Ampicillin (Sigma Aldrich, Milan, Italy) and grown until 600nm optical density reached 0.6-0.8. Induction of protein expression was performed adding 0.4 mM IPTG (Sigma Aldrich, Milan, Italy) to the culture, then grown for 2 hours. Pelleted cells were lysed in 1% Triton X-100 (Sigma Aldrich, Milan, Italy) in PBS 1X and were sonicated. Supernatants were incubated with 50 µl of Glutathione Sepharose 4B (GE Healthcare, Milan, Italy) 50% slurry. Following 3 washes with PBS 1X, the proteins were eluted in Protein Sample Buffer (Biorad, Segrate, Italy) and GST an GST-fusion proteins expression was evaluated by SDS-page using Stain Free Gels (Biorad, Segrate, Italy). The putative interactor proteins GABARAP,

GATE16, BNIP3, BNIP3L, in fusion with a Flag-tag, were in-vitro transcribed and translated, taking advantage of the TnT T7 Coupled Reticulocytes Lysate System (Promega, Milan, Italy) and the expression was checked by SDS page and Western Blot using the anti-Flag antibody (Sigma Aldrich, Milan, Italy). For interaction assay, a quantity of glutathione sepharose expressing cytoCDH6, deleted cytoCDH6 or only GST corrisponding to 1 µg of protein was mixed to 5-20 µl of in-vitro expressed putative Interactors, Glutathione Sepharose 50% slurry up to 40 µl in Interaction Buffer to a final volume of 150 µl. Reactions were incubated at 4°C for 2 hours on a wheel, centrifugated at 2000 rpm for 1 minute at 4°C and the supernatant discarded. Following 2 washes with Interaction Buffer, Glutathione Sepharose was resuspended in 20 µl of Sample Buffer 2X. Samples were charged on gel (GST diluted 1:100, GST-citoCDH6 1:10) for SDS page. Western Blot was performed using anti Flag antibody.

Interaction Buffer:
Hepes pH 7.8   20mM
Kcl   150 mM
NP-40   0.02%
BSA   0.02 mg/ml
EDTA   2 mM
DTT   2 mM
Complete 7x Protease Inhibitor Cocktail (Roche, Monza, Italy)

RNA extraction, Reverse Transcriptase Reaction and quantitative real time-PCR

Total RNA extraction and purification was performed with RNAeasy Mini kit (Qiagen, Milan, Italy). 250 ng of RNA was retrotranscribed using the iScript cDNA kit (Biorad, Segrate, Italy). The engineered avian Reverse Transcriptase used has a reduced RNaseH activity and shows high thermal stability, producing high amounts of full-length cDNAs. Total RNA was mixed to 1 µl RT (RNase H+), 5X iScript Buffer (dNTPs, oligo (dt), random hexamers, RNAse inhibitors, $MgCl_2$ and stabilizers) and Nuclease free water to 20 µl final volume. The reaction was performed on a thermal

cycler with the following protocol: 5 minutes at 25°C (Priming), 1 hour at 45°C (Reverse Transcription) and 1 minute at 95°C (RT inactivation). The obtained cDNA was diluted 3times with Nuclease Free Water for qPCR. To perform qPCR, Sso Fast EvaGreen Super Mix (BioRad, Segrate, Italy), a ready to use 2X Mix containing all components except for template and primers, was used. 1 µl of diluted cDNA was mixed to 2X Sso Fast EvaGreen Mix (Sso7d-fusion Polymerase, EvaGreen dye, $MgCl_2$, dNTPs, stabilizers), 300 nM of each primer and nuclease free water to 10 µl. The detection was performed with the CFX96 Real Time PCR Detection System (BioRad, Segrate, Italy) following the protocol: 95°C for 30 sec, 95°C 5 sec, 59°C 5 sec for 40 cycles.. For relative target genes expression ΔΔCt was calculated normalizing to the geometric mean of three reference genes expression: Glyceraldehyde-3-phosphate dehydrogenase (*GAPDH*), CyclophilinA (*CYPA*) and Beta-D-Glucuronidase (*GUSB*), unless otherwise specified. Sequences of primers are listed in Table 7.

Scratch wound healing assay

24h after transfection, cells transfected with siCDH6 or siCTRL were seeded at 90% confluence in a 6-well plate in complete growth medium. 24 h after cell adhesion, scratches were applied using a cell scraper. Healing areas were captured at 0 and 24 h using a Nikon Ti-E inverted microscope (Nikon Instruments, Florence, Italy).

Cell Proliferation

$1*10^4$ cells for each cell line were seeded in triplicate (unless otherwise specified) in a 96 well plate in regular growth medium. Viable cells were counted after 24, 48 and 72 hours using trypan blue

(Sigma-Aldrich, Milan, Italy) staining and the Countess® Automated Cell Counter (Thermo Fisher Scientific, Monza, Italy).

MTT assay

The viability of cells transfected with siCTRL or siCDH6 was determined using the standard MTT [3-(4,5-dimethylthiazol-2-yl)-2,5-diphenyltetrazolium bromide] assay. The treatments were performed 48h after the transfection in 96 wells plate. The purple formazan crystals were dissolved in DMSO, transferred in a 96 well plate (100 μL/well), and the absorbance was recorded on a microplate reader at a wavelength of 570nm.

Invasion Chamber Assay

$5*10^4$ cells of each cell line, transfected 24 hours before with siCT or siCDH6, were seeded in Matrigel Invasion Chamber (BD Biosciences, San Jose, CA) in triplicate. After 24 hours, invading cells were methanol fixed, stained with crystal violet and pictures were obtained using a Nikon Ti-E inverted microscope. Three fields for each well were captured and invading cells were manually counted.

Western Blot and Immunofluorescence

Total protein extracts were obtained using Passive Lysis Buffer (Promega, Milan, Italy) added with Complete 7x Protease Inhibitor Cocktail (Roche, Monza, Italy). SDS–PAGE was performed using Bio-Rad apparatus and Mini-Protean TGX pre-cast gels (Bio-Rad, Segrate, Italy). For Immunoblot detection anti-mouse or rabbit HRP-conjugated secondary antibodies (GE Healthcare, Piscataway, NJ) and Clarity ECL Western Blotting Substrate (Bio-Rad, Segrate, Italy) were used. Western blot

quantification was carried out taking advantage of Image J software. For immunofluorescence staining, cells seeded in Lab-Tek Chamber slides (Nunc; Roskilde, Denmark) in regular growth medium were fixed in 4% PFA (in PBS 1X) for 15 min at room temperature, permeabilized with 0.1% Triton (in PBS 1X) for 5 min, blocked with 20% FBS and 2% BSA (in PBS 1X) for 1 h, stained with the primary antibody. Secondary anti-mouse Alexa 488, anti-mouse Alexa 594 or anti-Rabbit Alexa 594 conjugated antibody (Thermo Fisher Scientific, Monza Italy) were used to reveal the staining.

To stain Actin filaments Alexa 488 conjugated Phalloidin (Thermo Fisher Scientific, Monza, Italy) was used, while mitochondria were stained with Mitotracker Red (Thermo Fisher Scientific, Monza, Italy) following manufacturer instructions. The following primary antibodies were used: mouse anti-FAK, mouse anti-phosphorilated-FAK (pY397), mouse anti-N-Cadherin, mouse anti-E-Cadherin, mouse anti-βCatenin (BD Bioscence, Milan, Italy), rabbit anti-ZO1 (Thermo Fisher Scientific, Monza, Italy), mouse anti-Flag M2, mouse anti-Actin (Sigma Aldrich, Milan, Italy), rabbit anti-phosphorilated-AKT (Ser473), rabbit anti-LC3A/B, rabbit anti-DRP1 (Cell Signalling, Euroclone, Milan, Italy) mouse anti-phosphorilated-ERK (Santa Cruz, DBA, Milan, Italy).

ChIP-seq

$1.7*10^7$ Nthy-ori-3,1 treated with TGFβ or not treated were retrieved and cross-linking was performed with 1% formaldehyde. Cells were lysed with Cell Lysis buffer (Tris 10mM pH 8; KCl 85mM; NP40 0.5%; PI) and nuclei were extracted using Nuclei Lysis Buffer (Tris 50 mM pH 8; EDTA 10mM; SDS 1%; PI). The obtained nuclei were sonicated for 10 cycles (30'' ON and 30'' OFF) to obtain fragments of 100-200 bp, using a Bioruptor Pico sonicator (Diagenode, Milan, Italy).

Chromatin diluted 1:10 in ChIP Dilution Buffer (SDS 0.01%; TRITON X-100 1.1%; EDTA 1.2 mM; Tris 16.7mM pH8; NaCl 167nM; PI) was precipitated with 20 µl Magna ChIP Protein G Magnetic Beads (Merck Millipore, Milan, Italy) and 1µg of H3K27ac (Abcam, Cambridge, UK) or Rabbit Igg (Santa Cruz, DBA, Milan, Italy) antibodies. For each experiment, 1% of chromatin before immune-precipitation was kept as input control. The immune-precipitated DNA was controlled by qPCR. Samples were quantified at Qubit (Thermo Fisher Scientific, Milan, Italy) and charged on Bioanalyzer (Agilent, Milan, Italy) to evaluate sizing, quantitation, and purity of the obtained DNA fragments. The library creation for ChIP-seq was performed following the TruSeq ChIP Sample Preparation protocol (Illumina, Milan, Italy) and using 5-10 ng ChIP DNA as starting material. Following quantification, End Repair was performed to convert the overhangs resulting from sonication into blunt ends. A single A nucleotide was then added to the 3' ends of the blunt ends to avoid their ligation and reduce the production of concatenated template. Multiple indexing adapters where then ligated to the DNA fragments ends to allow their hybridization onto a flow-cell. The ligation products were charged on agarose gel for electrophoresis and gel excision purification was performed to remove un-ligated adapters or dimers of adapters. Purified fragments with adapters were specifically enriched by PCR performed with PCR Primer Cocktail which anneals to adapters' ends. To preserve library representation 18 PCR cycles were programmed. The obtained libraries were validated with Qubit and Bioanalyzer. The libraries were normalized to 10 nM and pooled in equal volumes ready for cluster generation.

The samples in triplicate were charged on Illumina NextSeq500 (Illumina, Milan, Italy) and bioinformatical analysis of H3K27ac peak enrichment was performed following the pipeline depicted in Figure 23.
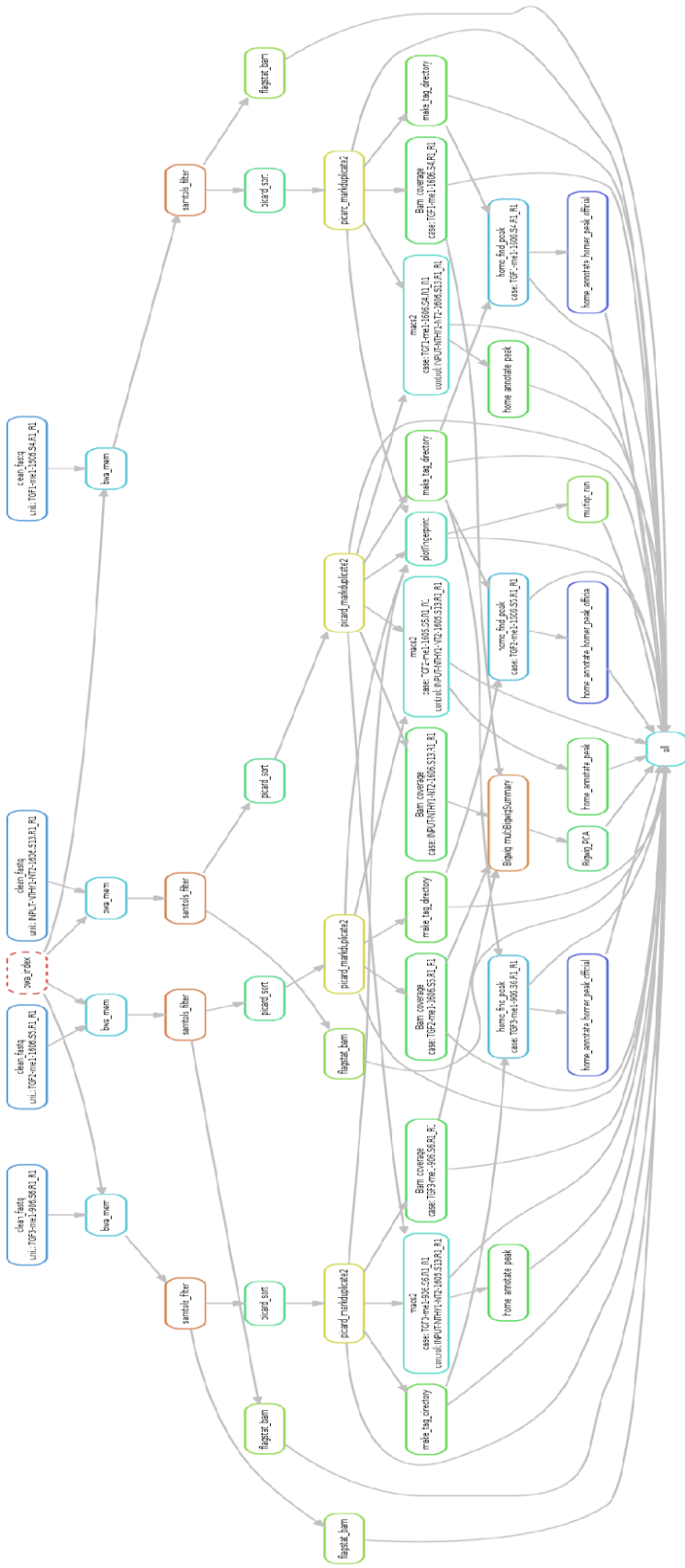
Figure 23. Schematic representation of the pipeline used for the bioinformatical analysis of ChIP-seq peak enrichment.

Lactate Production assay

To assay glycolytical rate of cell lines the bioluminescent Lactate-Glo assay was performed (Promega, Milan, Italy) following the Homogenous Assay protocol suggested. It couples lactate oxidation and NADH production with a system which take advantage of bioluminescent NADH detection. Lactate dehydrogenase converts lactate and NAD+ to pyruvate and NADH. When NADH is produced, a pro-luciferin Reductase Substrate is converted to luciferin, which produces light. The luminescent signal is proportional to the quantity of lactate present in the sample and increases until it is all consumed. $6*10^5$ BCPAP cells were plated in 6-well plate and transfected with scramble oligos (siCTRL) (Negative control Thermo Fisher Scientific, Monza, Italy) or a mix of 3 siRNA to target CDH6. After 24h $1.5*10^4$ BCPAP treated and Nthy-ori-3,1 were seeded in white 96 wells plates in complete medium. After 24h the cells were washed 3 times with PBS 1X and 40 µl of Glucose Free DMEM medium (Gibco, Thermo Fisher Scientific, Monza, Italy) supplemented with 5 mM Glucose (Sigma Aldrich, Milan, Italy) was added to the wells. After 2 hours at 37°C 5% CO_2, 5 µl of Inactivation Solution (HCl 0.6 N) were added to the medium to stop the reaction, following 5 minutes on the shaker, 5 µl of Neutralization Solution (Tris 1M pH 10.7) were added to lyse the cell and mixed for 60 seconds. 50 µl of Lactate Detection Solution (Luciferin Detection Solution + Reductase + Reductase Substrate + Lactate Dehydrogenase + NAD) were added, and the plate incubated at RT for 1 hour. The luminescence was read at the GloMax Multi Detection System (Promega, Milan, Italy). Signal to background (S/B) was calculated dividing the mean signal obtained by the samples by the mean signals obtained for the negative controls. Signal to noise (S/N) was calculated dividing the net signal (S/B) by the standard deviation of the negative control. Before the experiments, a lactate titration curve was obtained performing two-fold serial dilutions of Lactate from 200 µM following then the standard Lactate Glo protocol.

75

Seahorse Mitostress assay

The Seahorse XF Cell Mito Stress Test was used to measure Oxigen Consumption Rate (OCR) and Extracellular Acidification Rate (ECAR) on BCPAP and Nthy-ori-3,1 cell lines. BCPAP cells were plated in 6-well plate and transfected with scramble oligos (siCT) (Negative control Thermo Fisher Scientific, Monza, Italy) or a mix of 3 siRNAs to target CDH6 expression. After 24h, $2,5*10^5$ BCPAP siCT or siCDH6 and Nthy-ori-3,1 were seeded in Seahorse XF Cell Culture Microplates in 100 µl of complete medium. 12-16h before the experiment the Seahorse XF Cartridge was hydrated in Seahorse XF Calibrant (Agilent, Milan, Italy) at 37°C in an incubator without CO_2 overnight. 24h after cells' seeding the cells were washed two times with 1 ml of Seahorse XF Base medium added with 1 mM pyruvate, 2 mM glutamine and 10 mM glucose freshly prepared, equilibrated to 37°C and adjusted to pH 7.4. Performed the last wash, all medium was removed and 525 µl of medium were added. The plate was kept at 37°C without CO_2 for at least one hour. In the meantime, the XF Cartridge was prepared adding 75 µl of 8X Oligomycin, 9X FCCP, 10X Rotenone,11X Antimycin A in the ports A- B- C- D respectively. Each component at the concentration of 1µM in the final volume, except for the FCCP for the BCPAP cell line which was used at 0,2 µM, after performing a titration curve (concentration 0,1 – 2 µM). The cartridge was load on the Seahorse XF^e 24 instrument for calibration (pH and O_2 check). The cell plate was loaded on the instrument and the the assay started. The Seahorse data were normalized for cell number with SRB (Sulforhodamine B) assay and for mitochondria-indipendent OCR, subtracting the mean of OCR values obtained following Antimycin injection to all the other values obtained in the measurement. SRB binds the basic amino acid residues of trichloroacetic acid(TCA)-fixed cells. 125 µl of TCA were added to the medium after Seahorse assay, and incubated 1 h at 4°C. 5 washes with distilled water were performed. Once dry, the cells were added with 50 µl of SRB (Sigma Aldrich, Milan, Italy) dye dissolved in 1% Acetic

Acid. After 30 minutes incubation, the cells were washed 5 times with 800 µl of 1% Acetic Acid to eliminate the dye in excess. The dye in the cells were then eluted with Tris 10 mM pH 10.5 and the absorbance was read at 564 nm at GloMax-Multi Detection System (Promega, Milan, Italy).

Statistical analysis

Statistical analysis was performed with R Statistical Software (R Foundation for Statistical Computing, Vienne, Austria; http://www.R-project.org). Chi-squared test was used to compare frequencies between groups in Immunohistochemical staining. Clinicopathological parameters of patients were reported as frequencies or mean ± SD, ancd compared between immunohistological classes by Chi-Squared test and T-Test. Kaplan-Meier method was used to plot patients' survival curves with the log-rank statistics. All the in-vitro experiments were repeated at least 3 times and the results are reported as mean ± SD unless otherwise specified. Assumptions of each statistical test were verified. Threshold for significance was considered P-value <0.05.

Plasmid Constructs

A list of all constructs used is provided in Table 8. For GST-pulldown assay CDH6 interactors GABARAP, GATE16, and BNIP3L were amplified from the Yeast Two Hybrid-cDNA library and cloned into p3XFlag-CMV10 (Sigma Aldrich, Milan, Italy). BNIP3 gBlock Gene Fragment (IDT, Bologna) was cloned into p3Xflag-CMV10. The cytoplasmic region of CDH6 (cytoCDH6) was amplified from the Yeast Two Hybrid-cDNA library and cloned into pGEX-6P-1 (GE Healthcare, Milan), to be expressed in fusion with GST. cytoCDH6 LIR1, 2, 3 and 4 mutants were obtained by deletion of the four amino acid residues that constitute the domains. CytoCDH6 LIR 1, 2 or 3 domain

deletions were obtained by two consecutive amplification reactions. With the first amplification, two PCR products representing the regions flanking the sequence to be deleted were obtained. With the second amplification, the previously obtained PCR products were used as template for a PCR with the outermost primer pair. LIR 4 deletion was obtained with a single PCR with the reverse primer which binds the region upstream of the LIRmotif sequence. All the cytoCDH6 mutants were cloned in pGEX-6P-1 (pGEX-6P-1_cytoCDH6-LIR1-4). LC3 gBlock Gene Fragment (IDT, Bologna) was cloned into the pEGFP-C3 (Diatech Lab Line, Jesi) plasmid.

TABLE 7. Primers used in the study.

Primer	Sequence
Gabarap_HindIII_Fw	GATAAGCTTATGAAGTTCGTGGTACAAA
Gabarap_EcoRV_Rev	GTTGATATCTCACAGACCGTAGACACT
Gate16_HindIII_Fw	GATAAGCTTATGAAGTGGATGTTCAAG
Gate16_EcoRI_Rev	GATGAATTCTCAGAAGCCAAAAGTGTT
Bnip3L_HindIII_Fw	GATAAGCTTATGTCGTCCCACCTAGTC
Bnip3L_EcoRV_Rev	GTTGATATCTCAGTAGGTGCTGGCAGA
CDH6_KpnI_Fw	GTAGGTACCAGGCGGCAGCGAAAA
CDH6L_XhoI_Rev	CGCTCGAGTTAGGAGTCTTTGTCACTG
GST_cytoCDH6_Fw	GTACCCGGGCAGGCGGCAGCGAAAA
LIRmotif-1_Fw	CCGCCATACACTTACGCCTATGAAGGC
LIRmotif-1_Rev	GGCGTAAGTGTATGGCGGGGCAGTGGG
LIRmotif-2_Fw	CAAGACTATGACTGGGGACCTCGATTC
LIRmotif-2_Rev	TCCCCAGTCATAGTCTTGATCTGCATC
LIRmotif-3_Fw	CCTCGATTCGATATGTATGGAGGAGTG
LIRmotif-3_Rev	ATACATATCGAATCGAGGTCCCCAGTC
LIRmotif-4_XhoI_Rev	CGCTCGAGTTAGGAGTCTTTGTCACTG
T7_Koz_Fw	GGATCCTAATACGACTCACTATAGGGA
3xFlag_Rev	CGCCCCTCCTCTAGAGTCGAC
CDH6_Fw	TCACAGCCCAAGATCCAG

CDH6_Rev	TCTGTCCATATCTGTGTGTCGAT
Cyclophilin_Fw	GSCCCAACACAAATGGTTCC
Cyclophilin_Rev	TTTCACTTTGCCAAACACCA
CDH16_Fw	TGCAGAGCTGTCTGTGGAAG
CDH16_Rev	CCCCTGACAGCACGATCT
BNIP3_Fw	CGGGATGCAGGAGGAGAG
BNIP3_Rev	TAGAAACCGAGGCTGGAACG
BNIP3L_Fw	CAGCAGGGACCATAGCTCTC
BNIP3L_Rev	TGATACCCAGTCCGCACTTT
DRP1_Fw	GCTGCCTCAAATCGTCGTAG
DRP1_Rev	AGGTCTCCGGGTGACAATTC
FIS1_Fw	TTACGTCTTCTACCTGGCCG
FIS1_Rev	GTTCCTTGGCCTGGTTGTTC
MFN1_Fw	AGGATTTCATGCAAGATTACAGGA
MFN1_Rev	GCTCTGATAGTGTGCTGTTCG
OPA1_Fw	GCGGGATGTGGCGACTAC
OPA1_Rev	TCCTTTTATTCCAGAGCTGTGT
PINK1_Fw	CTGGGGAGTATGGAGCAGTC
PINK1_Rev	GAGAACCCGGATGATGTTGG
TAZ_Fw	CCCCTCATCACCGTGTCC
TAZ_Rev	CAGATGTGGCGGAGTTTCAG

TABLE 8. Constructs used in the study.

p3XFlagCMV10_GABARAP
p3XFlagCMV10_GATE16
p3XFlagCMV10_BNIP3
p3XFlagCMV10_BNIP3L
pEGFP-C3_LC3B
pGEX-6P-1
pGEX-6P-1_cytoCDH6
pGEX-6P-1_cytoCDH6-LIR1
pGEX-6P-1_cytoCDH6-LIR2
pGEX-6P-1_cytoCDH6-LIR3
pGEX-6P-1_cytoCDH6-LIR4

<u>Bibliography</u>

1. Howlader N, Noone AM, Krapcho M, Garshell J, Miller D, Altekruse SF, Kosary CL, Yu M, Ruhl J, Tatalovich Z,Mariotto A, Lewis DR, Chen HS, Feuer EJ, Cronin KA (eds). SEER Cancer Statistics Review, 1975-2012, National Cancer Institute. Bethesda, MD, http://seer.cancer.gov/csr/1975_2012/, SEER web site, April 2015.

2. Lloyd RV, Osamura RY, Kloppel G, Rosai J editors. World Health Organization Classification of Tumors of Endocrine Organs 4th edition. 2017.

3. Davies L, Morris LGT, Haymart M, Chen AY, Goldenberg D, Morris J, Ogilvie JB, Terris DJ, Netterville J, Wong RJ, Randolph G. American Association of Clinical Endocrinologist and American College of Endocrinology Disease State clinical review: the increasing incidence of thyroid cancer. Endocr Pract. 2015 Jun;21(6):686-96.

4. Kondo T, Ezzat S & Asa S. Pathogenetic mechanisms in thyroid follicular-cell neoplasia. Nature Reviews. Cancer 2006 6 292–306. doi:10.1038/nrc1836.

5. Brignardello E, Gallo M, Baldi I, et al. Anaplastic thyroid carcinoma:clinical outcome of 30 consecutive patients referred to a single institution in the past 5 years. 2007 Eur J Endocrinol 156:425-30

6. Dhillon AS, Hagan S, Rath O, et al. MAP kinase signalling pathways in cancer. Oncogene 2007; 26:3279–90.

7. Gandolfi G, Sancisi V, Piana S, Ciarrocchi A. Time to re-consider the meaning of BRAF V600E mutation in papillary thyroid carcinoma. 2015. Int J Cancer. 1;137(5):1001-11. doi: 10.1002/ijc.28976.

8. Davies L, Welch HG 2010 Thyroid cancer survival in the United States: observational data from 1973 to 2005. Arch Otolaryngol Head Neck Surg 136:440–444.

9. Cooper DS, Doherty GM, Haugen BR, Kloos RT, Lee SL, Mandel SJ, Mazzaferri EL, McIver B, Sherman SI, Tuttle RM 2006 Management guidelines for patients with thyroid nodules and differentiated thyroid cancer. Thyroid 16:109–142.

10. Haugen BR, Alexander EK, Bible KC, Doherty GM, Mandel SJ, Nikiforov YE, Paciniet F et. al. American Thyroid Association Management Guidelines for Adult Patients with Thyroid Nodules and Differentiated Thyroid Cancer: The American Thyroid Association Guidelines Task Force on Thyroid Nodules and Differentiated Thyroid Cancer. 2015.

11. The Cancer Genome Altlas Research Network. Integrated Genomic Characterization of Papillary Thyroid Carcinoma. Cell. Volume 159, Issue 3, 23 October 2014, Pages 676-690.

12. Nikiforov YE, Nikiforova MN. Molecular genetics and diagnosis of thyroid cancer. Nat Rev Endocrinol. 2011 Aug 30;7(10):569-80. doi: 10.1038/nrendo.2011.142.

13. de Biase D, Gandolfi G, Ragazzi M, Eszlinger M, Sancisi V, Gugnoni M, Visani M, Pession A, Casadei G, Durante C, Costante G, Bruno R, Torlontano M, Paschke R, Filetti S, Piana S, Frasoldati A, Tallini G, Ciarrocchi A. TERT Promoter Mutations in Papillary Thyroid Microcarcinomas.Thyroid. 2015 Sep;25(9):1013-9. doi: 10.1089/thy.2015.0101.

14. Gandolfi G, Ragazzi M, de Biase D, Visani M, Zanetti E, Torricelli F, Sancisi V, Gugnoni M, Manzotti G, Braglia L, Cavuto S, Merlo DF, Tallini G, Frasoldati A, Piana S and Ciarrocchi A. Genome-wide profiling identifies the THYT1 signature as a distinctive feature of widely metastatic Papillary Thyroid Carcinomas. 2017. Oncotarget. https://doi.org/10.18632/oncotarget.22805.

15. Kalluri R. EMT: When epithelial cells decide to become mesenchymal-like cells. J Clin Invest. 2009 Jun 1; 119(6): 1417–1419. doi: 10.1172/JCI39675.

16. Thiery JP. Epithelial-mesenchymal transitions in tumour progression. Nat Rev Cancer. 2002;2(6):442–54.

17. Tian M, Neil JR, Schiemann WP.Transforming Growth Factor-β and the Hallmarks of Cancer. Cell Signal. 2011 Jun;23(6):951-62. doi: 10.1016/j.cellsig.2010.10.015.

18. Gugnoni M, Sancisi V, Manzotti G, Gandolfi G and Ciarrocchi A. Autophagy and epithelial–mesenchymal transition: an intricate interplay in cancer. Cell Death and Disease. 2016. 7,e2520; doi:10.1038/cddis.2016.415.

19. Ismail Sahin Gu et al evolution and diversity of cadherins and catenins. 2017. Exp.cell.res. 358(1):3-9. doi: 10.1016/j.yexcr.2017.03.001.

20. Hulpiau P, van Roy F. Molecular evolution of the cadherin superfamily. Int J Biochem Cell Biol. 2009 Feb;41(2):349-69. doi: 10.1016/j.biocel.2008.09.027.

21. Yoshida C, Takeichi M. Teratocarcinoma cell adhesion: identification of a cell-surface protein involved in calcium-dependent cell aggregation. Cell. 1982 Feb;28(2):217-24.

22. Coopman, P. J., Do, M. T., Thompson, E. W., & Mueller, S. C. Phagocytosis of cross-linked gelatin matrix by human breast carcinoma cells correlates with their invasive capacity. 1998. Clin Cancer Res, 4, 507–515.

23. Jeanes A, Gottardi CJ & Yap AS Cadherins and cancer: how does cadherin dysfunction promote tumor progression? 2008. Oncogene 27, 6920–6929.

24. Takeichi M. Cadherins in cancer: implications for invasion and metastasis Curr. Opin. Cell Biol., 5. 1993, pp. 806-811.

25. Berx, G. & van Roy, F. Involvement of members of the cadherin superfamily in cancer. 2009.Cold Spring Harb. Perspect. Biol. 1, a003129.

26. Lammens T, Swerts K, Derycke L, De Craemer A, De Brouwer S, De Preter K, Van Roy N, Vandesompele J, Speleman F, Philippé J, Benoit Y, Beiske K, Bracke M, Laureys G. N cadherin in neuroblastoma disease: expression and clinical significance. PLoS One. 2012;7(2):e31206. doi: 10.1371/journal.pone.0031206.

27. Van Marck V, Stove C, Van Den Bossche K, Stove V, Paredes J, Vander Haeghen Y, Bracke M. P cadherin promotes cell–cell adhesion and counteracts invasion in human melanoma. Cancer Res. 2005 Oct 1;65(19):8774-83.

28. Bryan RT, Tselepis C. Cadherin switching and bladder cancer. J Urol. 2010 Aug;184(2):423-31. doi: 10.1016/j.juro.2010.04.016.

29. Giampietro C, Taddei A, Corada M, Sarra-Ferraris GM, Alcalay M, Cavallaro U, Orsenigo F, Lampugnani MG, Dejana E. Overlapping and divergent signaling pathways of N cadherin and VE cadherin in endothelial cells. Blood. 2012 Mar 1;119(9):2159-70. doi: 10.1182/blood-2011-09-381012.

30. Bartolomé RA, Barderas R, Torres S, Fernandez-Aceñero MJ, Mendes M, García-Foncillas J, Lopez-Lucendo M, Casal JI. Cadherin 17 interacts with α2β1 integrin to regulate cell proliferation and adhesion in colorectal cancer cells causing liver metastasis. Oncogene. 2014 Mar 27;33(13):1658-69. doi: 10.1038/onc.2013.117.

31. Andreeva, AV, Kutuzov MA. Cadherin 13 in cancer. Genes Chromosomes Cancer. 2010 Sep;49(9):775-90. doi: 10.1002/gcc.20787.

32. Li AM, Tian AX, Zhang RX, Ge J, Sun X, Cao XC. Protocadherin 7 induces bone metastasis of breast cancer. Biochem Biophys Res Commun. 2013 Jul 5;436(3):486-90. doi: 10.1016/j.bbrc.2013.05.131.

33. van Roy F. Beyond E cadherin: roles of other cadherin superfamily members in cancer. Nat Rev Cancer. 2014 Feb;14(2):121-34. doi: 10.1038/nrc3647.

34. Shimoyama Y, Gotoh M, Terasaki T, Kitajima M, Hirohashi S. Isolation and sequence analysis of human cadherin-6 complementary DNA for the full coding sequence and its expression in human carcinoma cells. Cancer Res., 1995 May 15;55(10):2206-11.

35. Cho EA, Patterson LT, Brookhiser WT, Mah S, Kintner C et al. Differential expression and function of cadherin-6 during renal epithelium development. 1998. Development. 125: 803-812. PubMed: 9449663

36. Inoue T, Chisaka O, Matsunami H, Takeichi M. Cadherin-6expression transiently delineates specific rhombomeres, other neural tube subdivisions, and neural crest subpopulations in mouse embryos. 1997. Dev Biol 183: 183-194. doi:10.1006/dbio.1996.8501.

37. Paul R, Ewing CM, Robinson JC, Marshall FF, Johnson KR, Wheelock MJ, Isaacs WB. Cadherin-6, a Cell Adhesion Molecule Specifically Expressed in the Proximal Renal Tubule and Renal Cell Carcinoma. Cancer Res. 1997 Jul 1;57(13):2741-8.

38. Köbel M, Kalloger SE, Boyd N, McKinney S, Mehl E et al. Ovarian carcinoma subtypes are different diseases: implications for biomarker studies. 2008. PLOS Med 5: e232. doi:10.1371/journal.pmed.

39. Paul R, Necknig U, Busch R, Ewing CM, Hartung R et al. Cadherin-6: a new prognostic marker for renal cell carcinoma. 2004. J Urol 171: 97-101. doi:10.1097/01.ju.0000101512.47242.79. PubMed: 14665853.

40. Walker G, MacLeod K, Williams AR, Cameron DA, Smyth JF and Langdon SP. Estrogen-regulated gene expression predicts response to endocrine therapy in patients with ovarian cancer. Gynecologic oncology. 2007; 106:461-468.

41. Chalmers IJ, Hofler H, Atkinson MJ. Mapping of a cadherin gene cluster to a region of chromosome 5 subject to frequent allelic loss in carcinoma. 1999. Genomics 1;57(1): 160-163

42. Sancisi V, Gandolfi G, Ragazzi M, Nicoli D, Tamagnini I, Piana S, Ciarrocchi A. Cadherin 6 Is a New RUNX2 Target in TGF-β Signalling Pathway. PLoS One. 2013 Sep 12;8(9):e75489. doi: 10.1371/journal.pone.0075489.

43. Sancisi V, Borettini G, Maramotti S, Ragazzi M, Tamagnini I, Nicoli D, Piana S, Ciarrocchi A. Runx2 Isoform I Controls a Panel of Proinvasive Genes Driving Aggressiveness of Papillary Thyroid Carcinomas. J Clin Endocrinol Metab. 2012 Oct;97(10):E2006-15. doi: 10.1210/jc.2012-1903.

44. Tojkander S, Gateva G, Lappalainen P. Actin stress fibers—assembly, dynamics and biological roles. J Cell Sci 2012; 125: 1855–1864.

45. Hartsock A and Nelson WJ Adherens and Tight Junctions: Structure, Function and Connections to the Actin Cytoskeleton. Biochim Biophys Acta. 2008 Mar;1778(3):660-9.

46. Calì G, Gentile F, Mogavero S, Pallante P, Nitsch R, Ciancia G, Ferraro A, Fusco A, Nitsch L. CDH16/Ksp-Cadherin Is Expressed in the Developing Thyroid Gland and Is Strongly Down-Regulated in Thyroid Carcinomas. Endocrinology. 2012 Jan;153(1):522-34. doi: 10.1210/en.2011-1572.

47. Schaaf MB, Keulers TG, Vooijs MA, Rouschop KM. LC3/GABARAP family proteins: autophagy-(un)related functions. FASEB J. 2016 Dec;30(12):3961-3978.

48. Kim H, Rafiuddin-Shah M, Tu HC, Jeffers JR, Zambetti GP, Hsieh JJ, et al. Hierarchical regulation of mitochondrion-dependent apoptosis by BCL-2 subfamilies. Nat Cell Biol. 2006;8(12):1348–58.).

49. Kabeya Y, Mizushima N, Ueno T, Yamamoto A, Kirisako T, Noda T, Kominami E, Ohsumi Y and Yoshimori T. LC3, a mammalian homologue of yeast Apg8p, is localized in autophagosome membranes after processing. 2000. EMBO J. 19, 5720–5728.

50. Levine B, Kroemer G. Autophagy in the pathogenesis of disease. Cell. 2008; 132:27–42.

51. Wang J, Whiteman MW, Lian H, Wang G, Singh A, Huang D, Denmark T A non-canonical MEK/ERK signaling pathway regulates autophagy via regulating Beclin 1 J Biol Chem. 2009 Aug 7;284(32):21412-24. doi: 10.1074/jbc.M109.026013.

52. Poole AC, Thomas RE, Andrews LA, McBride HM, Whitworth AJ, Pallanck LJ. The PINK1/Parkin pathway regulates mitochondrial morphology. Proc Natl Acad Sci U S A. 2008 Feb 5;105(5):1638-43. doi: 10.1073/pnas.0709336105.

53. Buhlman L, Damiano M, Bertolin G, Ferrando-Miguel R, Lombès A, Brice A, Corti O. Functional interplay between Parkin and Drp1 in mitochondrial fission and clearance. Biochim Biophys Acta. 2014 Sep;1843(9):2012-26. doi: 10.1016/j.bbamcr.2014.05.012.

54. Mishra P, David CC. Metabolic regulation of mitochondrial dynamics. 2016. JCB. 212 (4): 379. Doi: 10.1083/jcb.201511036.

55. Wild P, McEwan DG, Dikic I The LC3 interactome at a glance. J Cell Sci. 2014 Jan 1;127(Pt 1):3-9. doi: 10.1242/jcs.140426.

56. An integrated encyclopedia of DNA elements in the human genome The ENCODE Project Consortium Nature 489, 57–74 . 06 September 2012.

57. Heintzman, N. D., Stuart, R. K., Hon, G., Fu, Y., Ching, C. W., Hawkins, R. D. et al. Distinct and predictive chromatin signatures of transcriptional promoters and enhancers in the human genome. Nat. Genet. 2007. 39, 311–318.

58. Spicuglia, S, Vanhille, L. Chromatin signatures of active enhancers. Nucleus.2012. 3, 126–131.

59. Morris KV, Mattick JS. The rise of regulatory RNA. Nature reviews Genetics. 2014;15:423-437.

60. Anastasiadou E, Jacob LS, Slack FJ Non-coding RNA networks in cancer. Nat Rev Cancer. 2017 Nov 24. doi: 10.1038/nrc.2017.99.

61. Wei Su1, Shibao Li, Xiaofan Chen, Lingyu Yin, Ping Ma, Yingyu Ma, Bing Su. GABARAPL1 suppresses metastasis by counteracting PI3K/Akt pathway in prostate cancer. Oncotarget. 2017 Jan 17; 8(3): 4449–4459.

62. Catalano M, D'Alessandro G, Lepore F, Corazzari M, Caldarola S, Valacca C et al. Autophagy induction impairs migration and invasion by reversing EMT in glioblastoma cells. Mol Oncol 2015; 9: 1612–1625.

63. Akalay I, Janji B, Hasmim M, Noman MZ, Andre F, De Cremoux P et al. Epithelial-tomesenchymal transition and autophagy induction in breast carcinoma promote escape from T-cell-mediated lysis. Cancer Res 2013; 73: 2418–2427.

64. Peng YF, Shi YH, Ding ZB, Ke AW, Gu CY, Hui B et al. Autophagy inhibition suppresses pulmonary metastasis of HCC in mice via impairing anoikis resistance and colonization of HCC cells. Autophagy 2013; 9: 2056–2068.

65. Milner DJ, Mavroidis M, Weisleder N, Capetanaki Y. Desmin cytoskeleton linked to muscle mitochondrial distribution and respiratory function. J Cell Biol 2000;150: 1283.

66. Liu CY, Lin HH, Tang MJ, Wang YK. Vimentin contributes to epithelial-mesenchymal transition cancer cell mechanics by mediating cytoskeletal organization and focal adhesion maturation. Oncotarget 2015; 6: 15966–15983.

67. Klymkowsky MW, Savagner P. Epithelial-mesenchymal transition: a cancer researcher's conceptual friend and foe. Am J Pathol. 2009. 174: 1588-1593. doi:10.2353/ajpath.2009.080545. PubMed: 19342369.

68. Tsuji T, Ibaragi S, Hu GF. Epithelial-mesenchymal transition and cell cooperativity in metastasis. Cancer Res. 2009 Sep 15;69(18):7135-9. doi: 10.1158/0008-5472.CAN-09-1618.

69. Revenu C, Gilmour D. EMT 2.0: shaping epithelia through collective migration. Curr Opin Genet Dev. 2009 Aug;19(4):338-42. doi: 10.1016/j.gde.2009.04.007.

70. Friedl P, Locker J, Sahai E, Segall JE. Classifying collective cancer cell invasion. Nat Cell Biol. 2012 Aug;14(8):777-83. doi: 10.1038/ncb2548. Review. PMID: 22854810.

71. Choi PW, Yang J, Ng SK, Feltmate C, Muto MG, Hasselblatt K, Lafferty-Whyte K, JeBailey L, MacConaill L, Welch WR, Fong WP, Berkowitz RS, Ng SW. Loss of E-cadherin disrupts ovarian epithelial inclusion cyst formation and collective cell movement in ovarian cancer cells. Oncotarget. 2016 Jan 26;7(4):4110-21. doi: 10.18632/oncotarget.6588.

72. Gomes LC, Scorrano L. Mitochondrial morphology in mitophagy and macroautophagy. Biochim Biophys Acta 2013; 1833: 205–212.

73. Desai SP, Bhatia SN, Toner M, Irimia D. Mitochondrial localization and the persistent migration of epithelial cancer cells. Biophys J. 2013; 104: 2077–2088.

74. Anesti V, Scorrano L. The relationship between mitochondrial shape and function and the cytoskeleton. Biochim Biophys Acta. 2006 May-Jun;1757(5-6):692-9.

75. Maes H, Van Eygen S, Krysko DV, Vandenabeele P, Nys K, Rillaerts K et al. BNIP3 supports melanoma cell migration and vasculogenic mimicry by orchestrating the actin cytoskeleton. Cell Death Dis. 2014; 5: e1127.

76. Esteban-Martínez L, Boya P. BNIP3L/NIX-dependent mitophagy regulates cell differentiation via metabolic reprogramming. Autophagy. 2017 Jun 14:0. doi: 10.1080/ 15548627.2017.1332567.

77. Rehman J, Zhang HJ, Toth PT, Zhang Y, Marsboom G, Hong Z et al. Inhibition of mitochondrial fission prevents cell cycle progression in lung cancer. FASEB J 2012;26: 2175–2186.

78. Xie Q, Wu Q, Horbinski CM, Flavahan WA, Yang K, Zhou W et al. Mitochondrial control by DRP1 in brain tumor initiating cells. Nat Neurosci 2015; 18: 501–510.

79. Zhao J, Zhang J, Yu M, Xie Y, Huang Y, Wolff DW et al. Mitochondrial dynamics regulates migration and invasion of breast cancer cells. Oncogene 2013; 32:4814–4824.

80. Kashatus JA, Nascimento A, Myers LJ, Sher A, Byrne FL, Hoehn KL et al. Erk2 phosphorylation of Drp1 promotes mitochondrial fission and MAPK-driven tumor growth. Mol Cell 2015; 57: 537–551.

81. O.Warburg, On the origin of cancer cells. Science. 1956. 123 (1956) 309–314.

82. W.H. Koppenol, P.L. Bounds, C.V. Dang, Otto Warburg's contributions to current concepts of cancer metabolism, Nat. Rev. Cancer 11 (2011) 325–337.

83. Danhier P, Bański P, Payen VL, Grasso D, Ippolito L, Sonveaux P, Porporato PE. Cancer metabolism in space and time: Beyond the Warburg effect. Biochim Biophys Acta. 2017 Aug;1858(8):556-572. doi: 10.1016/j.bbabio.2017.02.001.

84. Zacksenhaus E, Shrestha M, Liu JC, Vorobieva I, Chung PED, Ju Y, Nir U, Jiang Z. Mitochondrial OXPHOS Induced by RB1 Deficiency in Breast Cancer: Implications for Anabolic Metabolism, Stemness, and Metastasis. Trends Cancer. 2017 Nov;3(11):768-779. doi: 10.1016/j.trecan.2017.09.002.

85. Iyer MK, Niknafs YS, Malik R, Singhal U, Sahu A, Hosono Y et al. The landscape of long non coding RNAs in the human transcriptome. Nat Genet. 2015, 47, 199-208.

86. Batista PJand Chang HY. Long non-coding RNAs: cellular address codes in development and disease. Cell. 1993;152,1298-1307.

87. Schmitt AM, Chang HY. Long Noncoding RNAs: At the Intersection of Cancer and Chromatin Biology. Cold Spring Harb Perspect Med. 2017 Jul 5;7(7). pii: a026492. doi: 10.1101/cshperspect.a026492.

88. Nakato R and Shirahige K. Recent advances in ChIP-seq analysis: from quality management to whole-genome annotation. Brief Bioinform. 2017 Mar; 18(2): 279–290

89. Bialucha CU, Collins SD, Li X, Saxena P, Zhang X2, Dürr C, Lafont B, Prieur P, Shim Y, Mosher R, Lee D, Ostrom L, Hu T, Bilic S et al. Discovery and Optimization of HKT288, a Cadherin-6-Targeting ADC for the Treatment of Ovarian and Renal Cancers. Cancer Discov. 2017 Sep;7(9):1030-1045. doi: 10.1158/2159-8290.CD-16-1414.